Remote Sensing Applications: Society and Environment 41 (2026) 101847

Contents lists available at ScienceDirect

Remote Sensing Applications: Society and Environment

journal homepage: www.elsevier.com/locate/rsase

Spatiotemporal dynamics of carbon, water, and energy balance in Bangladesh using multi-source remote sensing and climate data

Nur Hussain [a,*], Md Saifuzzaman [b], Didar Islam [c], S.M. Shahriar Ahmed [d], Md Shamim Ahamed [e], Dara Shamsuddin [f]

[a] Department of Biology, University of Toronto, 3359 Mississauga Road, Mississauga, ON, L5L 1C6, Canada
[b] Department of Biology, McGill University, Montreal, QC, H3A 0G4, Canada
[c] Department of Geography and Planning, University of Saskatchewan, Saskatoon, SK, S7N 5C8, Canada
[d] Center for Environmental and Geographic Information Services (CEGIS), Dhaka, Bangladesh
[e] Department of Biological and Agricultural Engineering, University of California Davis, California, 95616, USA
[f] Department of Geography & Environment, Jahangirnagar University, Savar, Dhaka, 1342, Bangladesh

ARTICLE INFO

Keywords:
Carbon uptake
Energy balance
Light use efficiency
Gross primary productivity
Net ecosystem production

ABSTRACT

Exploring the complex interactions between climate variables and ecosystem processes is crucial for understanding long-term environmental changes. This study examines the spatiotemporal dynamics of carbon, water and energy fluxes and their impacts on ecosystem processes in Bangladesh from 2005 to 2022 utilizing multi-source remote sensing and ground-based meteorological data. Carbon dynamics are estimated through gross primary productivity (GPP), net primary production (NPP), and ecosystem respiration (RE). Water and energy balances are derived from evapotranspiration (ET), water use efficiency (WUE), net radiation (Rn), and latent heat (LE). Our estimates indicate that GPP varied from 2351.29 g C m^{-2} y^{-1} in 2009–2178.45 g C m^{-2} y^{-1} in 2020, while NPP ranged from 1248.13 g C m^{-2} y^{-1} in 2012 to 929.46 g C m^{-2} y^{-1} in 2020, reflecting temporal variations in photosynthetic efficiency and carbon storage. The ratio of LE/Rn was found to vary from 0.72 to 1.01, with an average of 83 %, indicating that a significant portion of the radiative energy was transferred to the atmosphere as turbulent flux. Validation of LUE-based GPP compared to FLUXCOM-GPP showed a moderate correlation ($R^2 = 0.61$, $p < 0.005$), supporting the reliability of the estimates. We also conducted multivariate regression analysis to assess the relationships between climate variables and carbon, water, and energy balance. The results indicate that photosynthetically active radiation (PAR) is the primary and dominant driver of GPP ($R^2 = 0.97$), while temperature and precipitation are key factors significantly influencing carbon uptake. This study presents a comprehensive, integrated assessment of carbon, water, and energy fluxes at the national scale across Bangladesh, emphasizing the crucial role of climate variables in shaping these fluxes and offering valuable insights for climate-resilient land management and sustainable carbon strategies in monsoon-dominated regions.

* Corresponding author.
E-mail addresses: nur.hussain@utoronto.ca, nurhussain55@gmail.com (N. Hussain), md.saifuzzaman@mail.mcgill.ca (M. Saifuzzaman), lwn608@usask.ca (D. Islam), shahriarbxd@gmail.com (S.M. Shahriar Ahmed), mahamed@ucdavis.edu (M. Shamim Ahamed), sdshamsuddin02@gmail.com (D. Shamsuddin).

https://doi.org/10.1016/j.rsase.2025.101847
Received 31 March 2025; Received in revised form 17 December 2025; Accepted 19 December 2025
Available online 27 December 2025

1. Introduction

Ecosystem functioning depends on the exchanges of carbon, water, and energy, and understanding these interactions is crucial in tropical regions vulnerable to climate extremes (Heimann and Reichstein, 2008; Malhi et al., 2020; Migliavacca et al., 2021; Pugnaire et al., 2019). These interactions are strongly influenced by seasonal climate variability, particularly the monsoon, which regulates water and energy dynamics into ecosystems (Kondo et al., 2017). Tropical monsoon climate plays a critical role in regulating vegetation phenology, water availability, and energy fluxes (Suepa et al., 2016). However, the insufficiency of long-term eddy covariance (EC) station-based flux measurement and site observed ecosystem data limit the ability to quantify ecosystem responses to climatic variability at a national scale in monsoon-affected regions (Rodda et al., 2021; Burman et al., 2025; Ma et al., 2025). Addressing this limitation requires an integrated approach that combines multi-source satellite remote sensing with climate records to monitor the spatiotemporal dynamics of carbon, water, and energy balance across diverse ecosystems (Deng et al., 2019; Bu et al., 2021).

Terrestrial ecosystems are the main carbon sinks, absorbing carbon dioxide (CO_2) through photosynthesis and storing it as biomass (Frank et al., 2015; Keenan and Williams, 2018; Ito, 2019; Yang et al., 2022; Nzabarinda et al., 2025). This process is commonly assessed using remote sensing indices such as the normalized difference vegetation index (NDVI) and leaf area index (LAI), which provide an indication of vegetation health and biomass productivity (Vicente-Serrano et al., 2016; Xue and Su, 2017; Gebrechorkos et al., 2023). LAI estimates vegetation cover per unit area (m^2/m^2), while gross primary productivity (GPP) quantifies carbon assimilation through photosynthesis (Asner et al., 2003; Yang et al., 2021; Röll et al., 2024). The balance between GPP, net ecosystem production (NEP), and ecosystem respiration (RE) determines whether ecosystems function as carbon sources or sinks and influences atmospheric CO_2 concentrations (Wang et al., 2021; Krause et al., 2022).

Carbon flux dynamics requires examining their interactions with energy and water cycles, which regulate ecosystem productivity (Govind and Kumari, 2014; Canadell et al., 2023). GPP characterizes the total carbon fixed through photosynthesis, while net primary production (NPP) accounts for the fraction remaining after plant respiration, supporting growth and biomass accumulation (Roxburgh et al., 2005; Van Oijen et al., 2010). The RE incorporates both autotrophic (plant) and heterotrophic (microbial) respiration, returning CO_2 to the atmosphere (Dusenge et al., 2019; Quetin et al., 2023). Traditionally, EC flux towers have been used to measure these fluxes in real time, providing crucial insights into carbon, water, and energy exchanges but their high cost and maintenance requirements of EC towers limit broader deployment (Baldocchi et al., 1988; Chu et al., 2021; Callejas-Rodelas et al., 2024), particularly in developing regions.

Energy balance is a key driver of ecosystem function, regulating interactions between terrestrial ecosystems and the atmosphere (Shaver et al., 2000; Smith et al., 2013). Energy exchange occurs through radiative and turbulent fluxes, with net radiation (Rn) and ground heat flux (G) representing energy absorbed by the land surface (Aguiar et al., 2019; Bhattacharya et al., 2022). Latent heat flux (LE) and sensible heat flux (H) determine how energy is partitioned into evapotranspiration (ET) and surface temperature regulation (Wilson et al., 2002; Sepulcre-Canto et al., 2014; Chen and Liu, 2020). The efficiency of these exchanges influences ecosystem productivity, resilience, and responses to environmental variability. Analyzing long-term variations in energy balance components (Rn, LE, H, and G) provides critical understanding into how ecosystems allocate energy and regulate carbon and water fluxes (D'Odorico et al., 2010). Besides, ET plays a key role in linking energy, water, and carbon cycles, representing water loss through plant transpiration and soil evaporation (Novák and Novák, 2012; Bu et al., 2021). Water use efficiency (WUE), defined as the ratio of GPP to ET, specifies an ecosystem's ability to sustain carbon uptake with minimal water loss (Yang et al., 2016; Liu et al., 2020; Elfarkh et al., 2023; Fathi-Taperasht et al., 2023). Higher WUE reflects improved drought resilience, while variations in ET and GPP highlight shifts in water availability and carbon assimilation (Seleiman et al., 2021; Sharma et al., 2023). Drought conditions disrupt this balance by reducing GPP, increasing water stress, and limiting carbon sequestration. Understanding the interplay between ET, GPP, and WUE is essential for evaluating ecosystem responses to climate variability and maintaining carbon, water and energy balance stability (Yang et al., 2021, 2024; Zhang et al., 2024).

The critical importance of carbon-water-energy interactions is well recognized; however, comprehensive research on these dynamics, particularly in the context of ecosystem functioning, is lacking in many regions. The present study focuses on Bangladesh, located in a tropical region in South Asia that is highly vulnerable to climate change and extreme weather events such as flooding, and prolonged droughts are common annual climatic phenomena (Azam et al., 2021; Islam et al., 2022; Das et al., 2024). Its monsoon-driven climate influences seasonal variations in vegetation productivity, water availability, and energy fluxes, which shape carbon dynamics. While agricultural lands, wetlands, forests, and coastal ecosystems contribute to regional and global carbon cycles, national-scale assessments of long-term carbon flux trends are limited. Very few studies have addressed the aspects of ecosystem functioning in relation to climate change, leaving a significant gap in understanding the broader spatial and temporal patterns of carbon uptake and ecosystem resilience (Ahmed et al., 1999; Reid and Shafiqul Alam, 2017; Majumder et al., 2019; Anjum et al., 2024; Bhowmik et al., 2024; Tithi et al., 2024). The present research conducts a comprehensive study integrating multi-source remote sensing and weather station-based carbon, water, and energy flux, providing a deeper understanding of how climate change influences ecosystem processes and dynamics.

Recent advancements in ecosystem modeling have introduced diverse approaches to quantify coupled carbon, water, and energy fluxes (Zhang et al., 2017; Hussain et al., 2024a). Statistical and machine learning models integrate satellite, meteorological, and eddy covariance (EC) data to estimate ecosystem productivity and respiration (Guan et al., 2021; Zhu et al., 2023; Ma et al., 2025). Light Use Efficiency (LUE) models describe GPP-based carbon dynamics as a function of absorbed photosynthetically active radiation (PAR) and environmental constraints such as temperature, vapor pressure deficit (VPD), and radiation (Guan et al., 2021; Hussain et al., 2024b), while process-based models simulate biophysical and biogeochemical exchanges between the land surface and atmosphere (Deng et al., 2019). Remote sensing provides a scalable, cost-effective means for monitoring carbon fluxes (Zhao et al., 2022; Hussain et al.,

2024a; Wang et al., 2024; Zhu et al., 2024), and integrating MODIS-derived GPP with PAR, NDVI, and climatic variables improves estimates of ecosystem productivity and carbon balance (Zhang et al., 2017, 2020; Guan et al., 2021; Weiland et al., 2023). Integration of multi-source GPP datasets (MODIS, GOSIF-GPP, and FLUXCOM) with EC flux measurements further enhances process-based estimation of carbon uptake and photosynthetic performance beyond traditional LUE models, supporting assessments of interannual variability and climatic stressors such as temperature, PAR, and precipitation on carbon–water–energy interactions (Li and Xiao, 2019).

The primary purpose of this study is to investigate long-term (2005–2022) carbon, water, and energy fluxes in Bangladesh using multi-source remote sensing data and climate records from weather stations. The specific objectives are: (i) to assess seasonal and interannual variations in biomass productivity using satellite-derived phenological indicators; (ii) to quantify the spatiotemporal dynamics of carbon, water, and energy fluxes across diverse tropical ecosystems; (iii) to investigate the role of key climatic drivers in regulating carbon uptake, evapotranspiration, and energy exchange processes. By examining the interactions between carbon, water, and energy fluxes, this study fills a significant knowledge gap by providing a comprehensive long-term assessment of ecosystem resilience and carbon sequestration potential in Bangladesh. Leveraging multi-source remote sensing with ground-based weather station data, this study provides enhanced spatial and temporal resolution compared with previous research in similar ecosystems (Burman et al., 2020, 2021, 2024, 2025; Dubey and Ghosh, 2023).

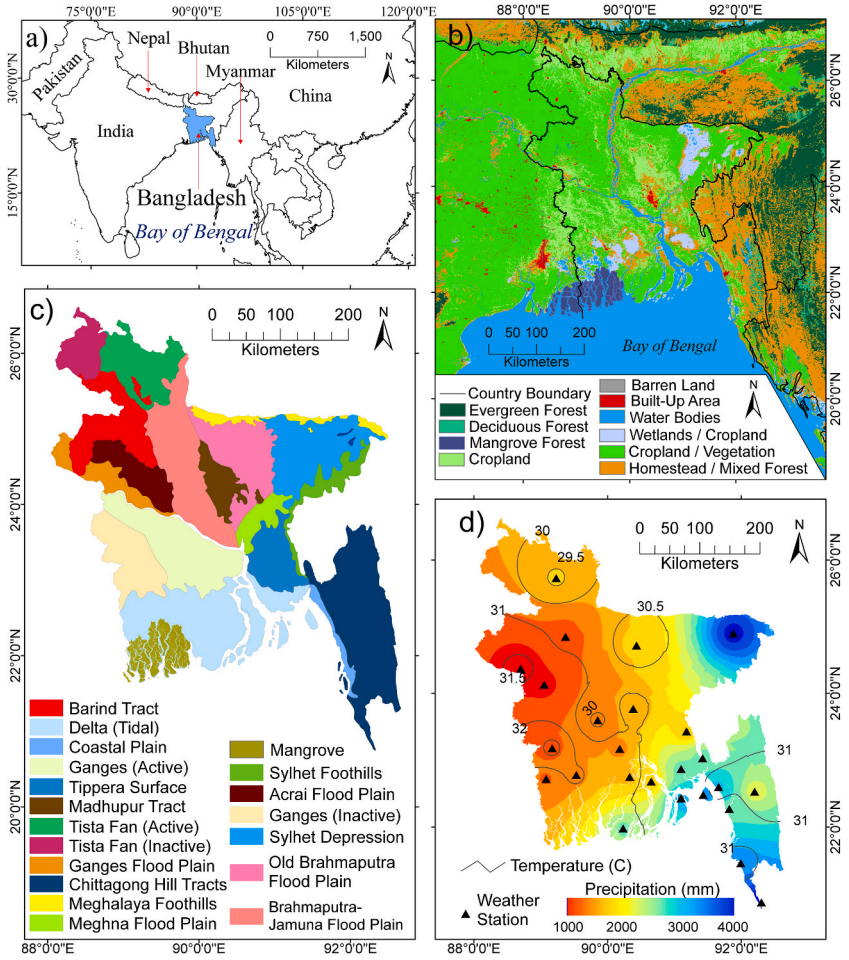

Fig. 1. Study Area Maps: (a) The location of Bangladesh; (b) Land Use/Land Cover (LULC) of Bangladesh, derived from MODIS-LULC data using the FAO land use classification system (Di Gregorio and Jansen, 2005); (c) Generalized Physiographic Map of Bangladesh, where major physiographic classes are categorized based on their geological and ecological characteristics (United States Geological Survey, 2021); and (d) Climate map of Bangladesh showing the locations of weather stations, with a color gradient representing average precipitation across the country from 2005 to 2022 and contour lines indicating temperature isotherms for the same period.

2. Data and methods

2.1. Study area

The study area, Bangladesh, is located in South Asia, spanning latitudes 20°34″ to 26°38″ N and longitudes 88°01″ to 92°41″ E, with a total land area of 148,460 km^2 (Central Intelligence Agency, 2025). The Bay of Bengal borders the country to the south and shares land boundaries with India on three sides, while a small portion of the southeast borders Myanmar (Fig. 1). Bangladesh is predominantly a low-lying floodplain, with its origins in the Himalayan Mountain range. Its geographic location makes it highly susceptible to the impacts of climate change (Islam et al., 2015). Bangladesh has a tropical humid climate characterized by moderate temperatures, high humidity, and notable fluctuations in air pressure, wind direction, rainfall, and temperature (Fattah et al., 2023). The average minimum temperature hovers around 15 °C, while maximum temperatures reach 35 °C during the hot summer. The country receives an average of 2300 mm of precipitation annually, with most rainfall occurring during the month of July. Bangladesh has three distinct agroclimatic seasons: (i) the hot pre-monsoon summer (March to May), (ii) the rainy monsoon summer (June to September), and (iii) the dry winter season (December to February). These seasonal climate variations and the country's physiographic features significantly influence agricultural productivity and vegetation growth (Hussain et al., 2021).

The ecosystem and vegetation distribution of Bangladesh is influenced by the physical characteristics of the Himalayan piedmont and the broader Indian subcontinental climate, which are also present in similar physiographic regions of India (Fig. 1). Moreover, the results of this study reflect broader trends applicable to similar climatic regions across the Indian subcontinent, highlighting the interconnected nature of carbon, water, and energy flux dynamics beyond national boundaries. However, Bangladesh was selected as the study area based on its dynamic vegetation types and seasonality, primarily due to data accessibility. This selection ensures a comprehensive analysis of carbon, water, and energy fluxes within a defined geopolitical region while accounting for the country's diverse microclimatic variations and environmental conditions.

2.2. Data

2.2.1. Remote sensing data

Satellite data from MODIS onboard Terra and Aqua were used, providing near-global coverage with 36 spectral bands at 250 m, 500 m, and 1000 m resolutions (Table 1). Data on PAR, NDVI, LAI, ET, GPP, land use and land cover (LULC), and land surface temperature (LST) were obtained from the MODIS data provider site (https://modis.gsfc.nasa.gov/data/; accessed on August 10, 2024). Energy flux data, including latent heat flux (LE), sensible heat flux (H) and ground heat flux (G), were sourced from NASA's Land Information System Data (LISD) of NASA GES-DISC at NASA Goddard Space Flight Center (https://disc.gsfc.nasa.gov/datasets/; accessed on August 20, 2024).

2.2.2. FLUXCOM and GOSIF GPP data

The FLUXCOM GPP dataset provides gap-filled, global gross primary productivity estimates derived from machine learning models trained on flux tower measurements and climate data (https://fluxcom.org/CF-Download/; accessed on July 25, 2025). The GOSIF GPP dataset offers satellite-based global GPP estimates derived from solar-induced chlorophyll fluorescence (SIF), providing high-resolution observations of photosynthetic activity (Li and Xiao, 2019). Both datasets were used to validate and compare the modeled GPP results.

Table 1
Summary of data characteristics. The study includes data from 25 weather stations across study area obtained from the Bangladesh Meteorological Department (BMD), with interpolation applied for comparison with satellite data at spatial scales ranging from 10 m to 500 m. The energy flux data including ground heat, sensible heat, and latent heat were sourced from the Land Information System Data (LISD) of NASA Goddard Space Flight Center.

Data Sources	Variable	Temporal Resolution	Spatial Resolution
Weather Stations (BMD)	Precipitation (mm) Temperature (°C) Humidity (%)	Monthly	500 m (Interpolated)
NASA – LISD; Version 2.0	Ground Heat (W m^{-2}) Sensible Heat (W m^{-2}) Latent Heat (W m^{-2})	Monthly	0.25° × 0.25°
MODIS (MCD18C2); Version 6.2	PAR (W m^{-2})	Daily	
MODIS (MOD13Q1); Version 6.1	NDVI	16-Days	
MODIS (MOD15A2H); Version 6.1	LAI (m^2/m^2)	16-Days	
MODIS (MOD16A2); Version 6.1	ET (mm d^{-1})	8-Days	
MODIS (MOD17A2H); Version 6.1	GPP (g Cm^{-2} d^{-8})	8-Days	
MODIS (MCD12Q1); Version 6.1	LULC	Yearly	
MODIS (MOD11A1); Version 6.1	LST (°C)	Daily	1 km
FLUXCOM	GPP (g C m^{-2} d^{-1})	Monthly	~8.5 km

2.2.3. Weather station data

Meteorological data, including temperature, precipitation, and wind speed, were collected from 25 ground stations of the Bangladesh Meteorological Department (BMD) for 2005–2022 and averaged by month. Station locations are shown in Fig. 1d, with distances between stations ranging from 27 km to 145 km (average 55 km). To match the 500 m resolution of MODIS satellite data, we interpolated the observations using the inverse distance weighting (IDW) tool in ArcGIS Pro 3.4 to create continuous climate surfaces. Climate variables were then extracted at the center of each MODIS grid cell to ensure spatial consistency. The mean temperature measured at weather stations was 30.7 °C, while the satellite-derived LST was 27.27 °C ($R^2 = 0.98$; $P < 0.0001$), and the mean monthly precipitation was 204.1 mm and 194.8 mm ($R^2 = 0.98$; $P < 0.0001$), indicating that both datasets captured temporal variability well (Hussain et al., 2025). Finally, the data were checked for consistency before and after interpolation. The interpolated temperature and precipitation maps are presented in the appendix (Figure A1).

2.3. Experimental design for ecosystem flux assessment

We used a comprehensive approach that combined satellite observations, empirical models, and ground-based meteorological data to quantify carbon, water, and energy fluxes across ecosystems. This enabled a thorough assessment of energy dynamics, water fluxes through evapotranspiration, and efficiency metrics, alongside key carbon processes like photosynthetic uptake, respiration, and net exchange (Wan, 2006;Running et al., 2019; Wang et al., 2024). This analysis was derived from multiple data sources, including MODIS satellite products, radiation flux data from NASA GES-DISC, and long-term meteorological records from national observatories. To ensure data quality and consistency, we applied rigorous pre-processing steps, such as quality control, gap filling, and spatial-temporal alignment.

All satellite imagery were preprocessed to convert top-of-atmosphere (TOA) data into surface-reflectance products prior to analysis. The preprocessing steps included radiometric calibration, atmospheric correction, cloud masking (cloud coverage less than 10 %) and geometric correction, following the standard methods provided by the respective data sources (Feng et al., 2012; Didan et al., 2015; Liang and Wang, 2017; Arsenault et al., 2018; Jung et al., 2020; Fathi-Taperasht et al., 2023). LST data were validated against nationwide weather station records from 2005 to 2022. The satellite-derived temperatures showed strong agreement with ground observations, with only a slight negative bias and a very high correlation ($R = 0.98$, $P < 0.0001$), confirming the reliability of the satellite LST for subsequent energy balance calculations.

Energy fluxes were estimated using the Penman–Monteith energy balance approach (Penman, 1948; Monteith, 1965) based on NASA-LISD datasets, which were preprocessed using land surface models (LSMs) and hydrologic models following the Land surface Data Toolkit (LDT) framework (Arsenault et al., 2018). Carbon flux validation was performed using the FLUXCOM framework, which

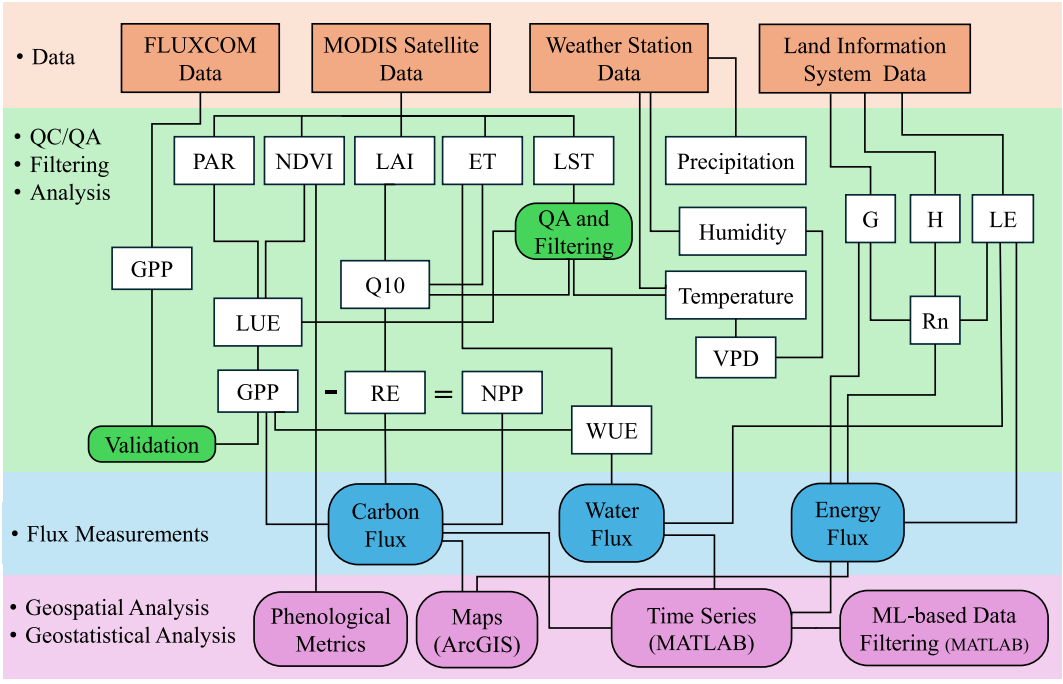

Fig. 2. Schematic representation of the experimental design, illustrating the integration of key variables used in the study. These include photosynthetically active radiation (PAR), normalized difference vegetation index (NDVI), leaf area index (LAI), evapotranspiration (ET), land surface temperature (LST), the water use efficiency (WUE), light use efficiency model (LUE), temperature sensitivity coefficient model (Q_{10}), gross primary production (GPP), ecosystem respiration (RE), and net primary production (NPP). Energy flux components are also depicted, where G represents ground heat flux, H denotes sensible heat flux, LE corresponds to latent heat flux, and Rn refers to net radiation.

applies a rescaling and flux estimation procedure and employs a hybrid machine-learning approach that combines random forests with simple decision stumps in the inner nodes and Gaussian process regression (GPR) in the leaf nodes to generate flux predictions (Jung et al., 2020). The processed datasets were integrated into a unified analytical framework, allowing us to examine ecosystem functioning and its responses to climate variability (Fig. 2).

2.4. Phenological metrics

We characterized the phenological phases of agricultural and forest ecosystems (deciduous and evergreen) using a threshold-based method with Land Use and Land Cover (LULC) data. Bangladesh's agricultural calendar includes two main growing seasons: Boro/Aus (winter crops) and Aman (monsoon crops), each exhibiting distinct photosynthetic activity levels. Forest ecosystems, including mixed-evergreen forests, homestead vegetation, and mangroves, as well as deciduous forests, demonstrate varying seasonal phenological patterns (Table 2). Vegetative ecosystem types in Bangladesh are classified into mixed-evergreen forests (hill forests), deciduous forests (Sal forests), and mangrove forests (Fig. 1b). This classification is based on data from the Department of Agricultural Extension (DAE), Dhaka, Bangladesh, and the Food and Agriculture Organization (FAO), Rome, Italy, with forest classifications drawn from the Forest Department (FD), Dhaka, Bangladesh, and additional insights from the Bangladesh Space Research and Remote Sensing Organization (SPARRSO) and the International Union for Conservation of Nature (IUCN) (Rahman, 2016).

In this study, 16-day interval NDVI data were interpolated to daily values and smoothed using a Savitzky–Golay filter with a third-degree polynomial and a 17-day window. These parameters were selected because monsoon climate regions are particularly affected by false seasonal signals caused by rapid vegetation changes and intermittent cloud cover. The 17-day window effectively reduces noise while preserving the true seasonal dynamics typical of double-cropping systems. Phenological metrics including Start of Season (SOS), Peak of Season (POS), and End of Season (EOS) were extracted from the smoothed NDVI using a threshold set at 30 percent ($\alpha = 0.3$) of the NDVI amplitude above the minimum baseline. Cao et al. (2018) used the threshold value of 0.9 for the correlation coefficient to select similar pixels for smoothing, whereas our study uses the 0.3 NDVI amplitude threshold to detect the SOS and EOS of vegetation activity. This threshold is commonly employed in agricultural studies to reliably identify the onset of greening while minimizing false detections caused by noise. It also aligns well with field-observed crop calendars in our monsoon croplands. These phenological metrics for the Boro and Aman seasons were derived following established methodologies (Zhang et al., 2003; White et al., 2005; Cao et al., 2018) and the regional crop calendar (Table 2).

$$\mathrm{NDVI}_{\mathrm{smoothed}}(t) = \sum_{k=-m}^{m} C_k \, NDVI\,(t+k) \tag{1}$$

$$T = NDVI_{min} + \alpha\,(NDVI_{max} - NDVI_{min}) \tag{2}$$

$$\mathrm{SOS} = \min\{t \in \mathrm{S} | \mathrm{NDVI}_{\mathrm{smoothed}}\,(\mathrm{t}) \geq \mathrm{T}\} \tag{3}$$

$$\mathrm{POS} = \mathrm{t} \in S_{max} NDVI_{\mathrm{smoothed}} \mathrm{NDVI}\,(\mathrm{t}) \tag{4}$$

$$\mathrm{EOS} = \max\{t \in \mathrm{S} | \mathrm{NDVI}_{\mathrm{smoothed}}\,(\mathrm{t}) \geq \mathrm{T}\} \tag{5}$$

where, t is the time (in days), C_k are the Savitzky–Golay filter coefficients computed based on polynomial fitting, $NDVI\,(t+k)$ represents the raw NDVI value at time $(t + k)$, T is the threshold value observed NDVI over the season, $NDVI_{min}$ and $NDVI_{max}$ are the minimum and maximum NDVI over the season, and α is the NDVI amplitude, SOS is Start of Season, the POS is Peak of Season and the EOS is End of Season.

Table 2
Vegetative ecosystem types in Bangladesh, including mixed-evergreen forests (hill forests), deciduous forests (Sal forests), and mangrove forests (both natural and planted).

Major LULC	Vegetation types	Photosynthesis level (Seasonality)
Agricultural crop	Boro	Low (April–May)
		High (Feb–Mar)
	Aus	Low (May–June)
		High (July)
	Aman	Low (July–Aug, Nov)
		High (Sep–Oct)
Forest	Mixed evergreen	Low (Nov–April)
		High (May–Oct)
	Deciduous	Low (Nov–April)
		High (May–Oct)
	Mangrove	High (Aug)
Homestead vegetation	Mixed evergreen	Low (Nov–April)
		High (May–Oct)

2.5. Calculating energy and water balance using remote sensing

The surface energy balance estimates the interaction between incoming and outgoing radiation, expressed through Rn and associated fluxes (Penman, 1948; Monteith, 1965). Rn, the total energy from incoming solar radiation, is determined by the difference between shortwave radiation and outgoing longwave radiation (Kalma, 1972). As the primary energy source, net radiation drives processes like evaporation, photosynthesis, and temperature regulation, influencing ET, carbon assimilation, and ecosystem productivity (Marcolla et al., 2020; Seneviratne et al., 2021). Rn is segregated into three key fluxes: LE, H and G (Bu et al., 2021). These fluxes provide insights into energy distribution within ecosystems, influencing both water and energy cycles (Zakariazadeh et al., 2024). The Penman-Monteith equation quantifies Rn to evaluate energy flow in the ecosystem (Penman, 1948; Monteith, 1965). Additionally, the carbon water and energy balance influences in the Vapor Pressure Deficit (VPD) and WUE. The VPD is calculated from weather station-based temperature and humidity data using Penman-Monteith equation (Penman, 1948, 1963; Monteith, 1965) and WUE is measured the ratio of GPP to ET, illustrating the efficiency of water in driving carbon uptake (Ai et al., 2020; Sett et al., 2023).

$$Rn = LE + H + G \tag{6}$$

$$WUE = \frac{GPP}{ET} \tag{7}$$

where Rn refers to net radiation (Wm^{-2}), LE corresponds to latent heat flux (Wm^{-2}), H denotes sensible heat flux (Wm^{-2}) and, G represents ground heat flux (Wm^{-2}), WUE is the water use efficiency ($gCm^{-2}mm$), ET is evapotranspiration and the GPP is the Gross Primary Production (gCm^{-2}) and ET is Evapotranspiration (mm).

2.6. Retrieval carbon balance using remote sensing

The carbon balance in ecosystems is modeled by the dynamic interplay between carbon fixation, release, and storage, expressed through the key indicators GPP, RE, and NPP. In this study, GPP was estimated using the LUE model, which links the PAR absorbed by vegetation to its efficiency in converting light into biomass (Monteith, 1972; Gower et al., 1999; Running et al., 2004). The model incorporates a conversion efficiency factor, the PAR in μmol, and the LUE, which varies with vegetation conditions (Zhang et al., 2017). PAR data were adjusted to reflect the fraction of radiation absorbed by the ecosystem. The LUE parameter was determined as a function of the NDVI, with LUE_{max} representing the maximum light use efficiency specific to the ecosystem type. RE was estimated using a modified Q10 temperature sensitivity model, which includes additional controls from ET and LAI (Delogu et al., 2017; Feng et al., 2018; Liu et al., 2024).

The Q10 metric quantifies the temperature sensitivity of biogeochemical processes with soil respiration exemplifying how its rate changes for every 10 °C increase in temperature. Across ecosystems ranging from forests and grasslands to croplands, Q10 values vary widely, reflecting differences in the sensitivity of soil CO_2 emissions to climatic drivers (Delogu et al., 2017; Feng et al., 2018). This sensitivity is strongly influenced by air temperature and precipitation, with higher Q10 values typically observed under cooler conditions and a decline in sensitivity as temperatures rise (Wang et al., 2006; Delogu et al., 2017). In this study, we applied the Q10 approach to evaluate the temperature sensitivity of soil respiration, following on methodologies from similar ecosystems, including temperate croplands (Delogu et al., 2017), grasslands (Feng et al., 2018), and tropical forests (Wang et al., 2006). This model accounts for the influence of temperature, vegetation conditions, and water availability on respiration rates (Davidson and Janssens, 2006; Delogu et al., 2017). The temperature sensitivity factor (Q10) was applied to the MODIS-LST and temperature data from weather stations (Weiland et al., 2023). Empirical coefficients for ET and LAI were set based on literature values (Monteith, 1972; Gower et al., 1999; Running et al., 2004; Zhang et al., 2017). These factors influence the rate of ecosystem respiration and were calculated for each time step.

Additionally, NEE was derived by subtracting GPP from RE, providing a measure of the net carbon flux in the ecosystem. Positive NEE values indicate carbon release, while negative values reflect carbon uptake by the ecosystem (See et al., 2024). NPP representing carbon fixed after accounting for autotrophic respiration, was calculated by subtracting RE from GPP. The following equations were used to compute these fluxes:

$$GPP = \alpha \times PAR \times LUE \tag{8}$$

$$LUE = LUE_{max} \times \frac{NDVI - NDVI_{min}}{NDVI_{max} - NDVI_{min}} \tag{9}$$

$$RE = (LUE_{max} + \beta \times ET + \gamma \times LAI) \times Q10^{(T - T_{ref})/10} \tag{10}$$

$$NPP = GPP - RE \tag{11}$$

Where, LUE is Light Use Efficiency, the equation estimates photosynthetic efficiency based on NDVI, maximum and minimum NDVI with LUE_{max} representing the maximum efficiency specific to the ecosystem is 0.42 (Zhang et al., 2017). It normalizes the difference between NDVI and its minimum value over the range between $NDVI_{max}$ and $NDVI_{min}$, allowing dynamic estimation of LUE, which

influences GPP. RE was estimated by combining maximum light use efficiency (LUE_{max}), evapotranspiration (ET), and leaf area index (LAI), while incorporating a temperature sensitivity factor (Q10) based on surface temperature sensitivity. Empirical coefficients $\beta = 0.5$ and $\gamma = 0.5$ were applied to weight the contributions of ET and LAI, reflecting the interaction of energy and water balance in regulating ecosystem respiration processes (Monteith, 1972; Gower et al., 1999; Running et al., 2004; Zhang et al., 2017). Finally, Net Primary Production (NPP) is calculated by subtracting RE from GPP, indicating the carbon available for plant growth, PAR is photosynthetically active radiation in μmol m^{-2} s^{-1} and α (alpha) is the conversion efficiency factor, determining the rate at which absorbed PAR is converted into carbon biomass of LAI extracted for different LULC.

Previous studies in South Asia have primarily relied on EC flux and satellite measurements to estimate carbon, water, and energy fluxes at the ecosystem scale (Table 3). While EC provides high-frequency, site-specific flux observations, its spatial coverage is restricted to individual tower footprints. In contrast, our study applies a LUE model combined with multi-source remote sensing (NDVI, LAI, ET) and ground-based weather data to estimate GPP. The correlation heatmap illustrates key relationships between environmental and ecosystem variables (Fig. 3a). To ensure reliability, our GPP estimates were compared with FLUXCOM-derived GPP, showing a satisfactory correlation ($R^2 = 0.61$, $p < 0.005$) along with which supports the robustness of the model–data approach for capturing national-scale carbon dynamics (Fig. 3b). Similarly, comparison with GOSIF GPP showed good agreement ($R^2 = 0.58$, $p < 0.005$) further validating the performance of the LUE-based GPP estimates (Fig. 3c).

2.7. Statistical analysis

This study included a dataset of 131,150,448 points per variable. To improve visualization and facilitate time-series generation, the dataset was reduced to 10,500 points for each month January from 2005 to December 2022 using machine learning techniques, optimizing computational efficiency while preserving analytical integrity. The reduced dataset retained statistical consistency with the raw data, showing similar mean and standard deviation values. This reduction was for visualization purposes only, with the full dataset used without any filtering for spatial analysis and map generation. The reduction process involved filtering and random sampling, following established methods (Olken and Rotem, 1995; Nagele, 2003; Khursheed et al., 2013).

$$X_i = \begin{cases} X_i & if\ X_i \notin [\mu X - 2\sigma X, \mu X + 2\sigma X] \wedge X_i \leq 0 \\ 0 & if\ X_i < 0 \\ NaN & if\ X_i \notin [\mu X - 2\sigma X, \mu X + 2\sigma X] \end{cases} \quad (12)$$

$$X_{filtered} = \sum_{i=1}^{X_{initial}} 1(X_1 \notin [\mu X - 2\sigma X, \mu X + 2\sigma X] \wedge X_i \leq 0) \quad (13)$$

$$X_{reduced} = X_{filtered}\left[r_1, r_2, \ldots\ldots, r_{n_{samples}}\right] \quad (14)$$

where, $\mu X \pm 2\sigma X$ were replaced with NaN, while values within the range were retained. The resulting subset, $X_{filtered}$, was reduced from 131,150,448 to 10,500 data points for each month January from 2005 to December 2022. The final subset, $X_{reduced}$, was obtained through random sampling.

We also performed single-variable linear regression to investigate relationships among the data variables. The correlation heatmap shows key interdependencies between environmental and ecosystem variables (Fig. 3a). Temperature shows moderate positive correlations with PAR (0.54) and Rn (0.75), and weaker correlations with VPD (0.24) and precipitation (0.48), while negatively correlating with WUE (−0.32). PAR strongly correlates with GPP (0.99) and VPD (0.81), highlighting seasonal patterns in photosynthesis. Rn is found highly correlated with precipitation (0.82), suggesting shared trends. VPD and precipitation are negatively correlated (−0.74), indicating that higher vapor pressure deficits are linked with lower precipitation. WUE strongly negatively correlates with ET

Table 3
Summary of studies on carbon, water, and energy balance across South Asian monsoon subtropical regions, including study focus, geographic setting, climate type, data sources, and estimated daily gross primary productivity (GPP) ranges. Approximate GPP values are extracted from published literature for comparative context.

Study Focus	Study Region	Climate	Data and Methods	Carbon Uptake (g C m^{-2} d^{-1})	Reference
Carbon balance	India	Humid Subtropical	Eddy Covariance	Daily GPP Range 0 to 20.	Burman et al. (2020)
Carbon and water exchanges	India	Humid Subtropical	Eddy Covariance	Approximate GPP Range 0 to 20.	Burman et al. (2021)
Carbon fertilization and ecological drought	India	Humid Tropical	ERA5/Earth System Model	Daily Standardized GPP Range 0 to 25.	Dubey and Ghosh (2023)
Carbon Water and Energy Balance	India	Humid Subtropical	Eddy Covariance	Approximate GPP Range 0 to 20.	Burman et al. (2024)
Carbon Water and Energy Balance	India	Humid Subtropical	Satellite data, Eddy Covariance	Daily GPP Range 0 to 20.	Burman et al. (2025)
Carbon Water and Energy Balance	Bangladesh	Tropical Humid	Satellite data, Light Use Efficiency	Daily GPP Range 0 to 15.	Present Study

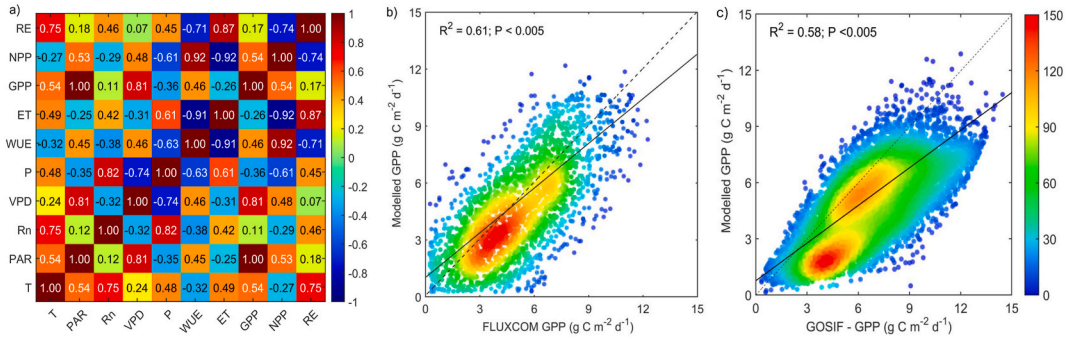

Fig. 3. (a) Correlation heatmap between climatic drivers and carbon, water, and energy fluxes using monthly averages from 2005 to 2022. Variables include Temperature (T), Photosynthetically Active Radiation (PAR), Net Radiation (Rn), Vapor Pressure Deficit (VPD), Precipitation (P), Water Use Efficiency (WUE), Evapotranspiration (ET), Gross Primary Production (GPP), Net Primary Production (NPP), and Ecosystem Respiration (RE). (b) Relationship between modeled GPP and FLUXCOM GPP, with point density indicated by the color gradient. (c) Comparison between GOSIF GPP and LUE-based GPP, with point density represented by a blue-to-red gradient, where red indicates higher density (0–500 points).

(−0.91) and positively with NPP (0.92), reflecting efficient water use in high-productivity ecosystems. ET negatively correlates with NPP (−0.92) and GPP (−0.26), indicating water limitations during high transpiration. RE shows weak correlations, except for positive associations with P (0.45) and ET (0.87). The heatmap illustrates the complex interactions between climate variables and ecosystem processes, highlighting how changes in one variable may affect others.

In addition, we examined the relationship between climatic variables and water, energy, and carbon balance through a Multiple Linear Regression (MLR) model, where climatic variables-such as temperature, precipitation, Rn, and PAR served as predictors. The model also included GPP, NPP, RE, and ET as dependent variables, as represented by Eq. (12) (Shewhart et al., 2003; Kutner et al., 2004)

$$Yi = \beta 0 + \beta 1 Xi1 + \beta 2 Xi2 + \cdots + \beta p Xip + \varepsilon i, i = 1, \cdots, n \tag{15}$$

where, *Yi* is the response variable, and *Xi*1, *Xi*2, …, *Xip*Xi1, Xi2, …, Xip are the predictor variables. $\beta 0$ is the intercept, and $\beta 1$, $\beta 2$, …, βpβ1, β2, …, βp are the coefficients that indicate the influence of each predictor on *Yi*. ϵi represents the error term, capturing the

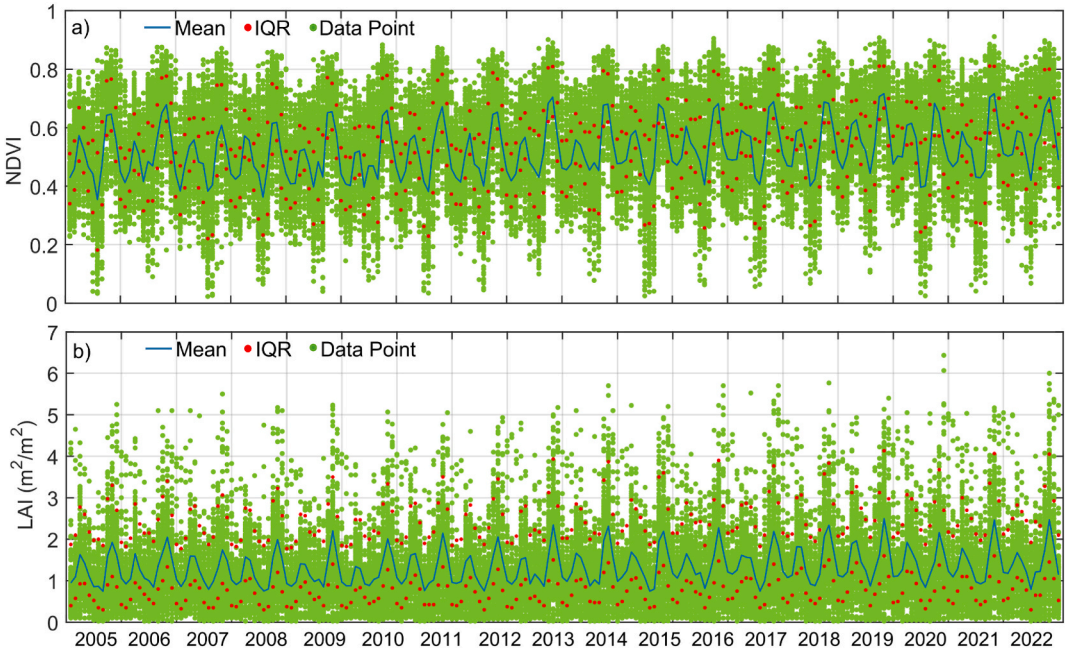

Fig. 4. Vegetation dynamics and biomass production time series. Monthly NDVI from 2005 to 2022 (panel a) illustrates seasonal cycles and interannual variations in vegetation health, while the monthly average LAI (panel b) over the same period reflects trends in vegetation density and biomass production. In both panels, the solid line represents the monthly mean, green dots indicate individual observations, and red dots show the interquartile range (IQR = Q3 − Q1) for each month, capturing the variability of the data.

difference between observed and predicted values. The model estimates these coefficients to minimize the error across all observations.

3. Results

3.1. Spatiotemporal dynamics of biomass production and seasonal phenological metrics

Analysis of NDVI and LAI from 2005 to 2022 reveals clear trends in vegetation health and biomass production in Bangladesh. The overall mean NDVI was 0.51 ± 0.08, gradually increasing from 0.49 in 2005 to 0.55 in 2022, with peaks in 2019 and 2022 (Fig. 4a). Monthly NDVI showed strong seasonal variability, peaking in September (0.63 ± 0.03) and October (0.66 ± 0.03) during the post-monsoon period, declining in the dry winter (December–February) and further reducing during the monsoon, particularly in June–July. Similarly, mean LAI increased from 1.28 ± 0.37 m^2/m^2 in 2005 to 1.49 ± 0.41 m^2/m^2 in 2022, with a peak of 1.57 ± 0.47 m^2/m^2 in 2019 (Fig. 4b). Monthly LAI was highest in September (1.73 ± 0.20 m^2/m^2) and October (2.22 ± 0.20 m^2/m^2) and lowest in June (1.03 ± 0.14 m^2/m^2) and July (0.94 ± 0.14 m^2/m^2), reflecting seasonal changes in vegetation density. These consistent patterns across NDVI and LAI highlight the strong influence of climatic seasonality on vegetation dynamics and biomass production.

The phenological phases of key crops in Bangladesh, namely Boro (winter crops) and Aman (monsoon crops), were analyzed for the period 2005 to 2022 to understand the timing of crop growth and the impacts of climatic factors on agricultural biomass productivity (Table 4). By applying a threshold-based method in combination with knowledge-based crop calendars and a Savitzky–Golay filter, the study calculated three key phenological metrics: the Start of Season (SOS), Peak of Season (POS), and End of Season (EOS) for each crop. The Boro and Aus crops typically began their growing season between early and mid-January, with POS occurring between late March and mid-April, and EOS in late June. For the Aman crop, SOS occurred between early and mid-July, POS from late September to mid-October, and EOS between late November and December. These phases were consistent across the study period, with slight annual variations due to climatic factors.

The observed interannual variations in SOS, POS, and EOS were largely influenced by changing climatic conditions, such as temperature and rainfall patterns, along with shifts in agricultural practices. The data revealed that the timing of each crop's growing season is closely tied to environmental factors, which have led to shifts in phenological phases over the years. Understanding these trends is crucial for improving agricultural practices, ensuring better crop management, and mitigating the impact of climate change on crop productivity in Bangladesh. Additionally, the winter season, with low temperatures and reduced precipitation, plays a significant role in Boro crops growth. However, these crops rely heavily on groundwater irrigation during the winter, which minimizes the impact of climatic factors such as soil moisture and precipitation on biomass growth. This reliance on groundwater not only buffers the crops from climatic fluctuations but also enhances water use efficiency, further optimizing growth despite challenging climatic conditions.

In addition, the phenological phases in Bangladesh over the period from 2005 to 2022 are mainly represented by two forest types, deciduous and evergreen, as summarized in Table 5. For deciduous forests, the SOS generally occurred in March or April, with the POS typically occurring between August and September. The EOS was observed consistently around the end of November to early December, marking the end of active growth. The timing of these phases showed minor variations from year to year, reflecting the impacts of climatic fluctuations, particularly temperature and precipitation patterns. In contrast, evergreen forests include tropical rain forest showed a more consistent phenological pattern across the years. The SOS for evergreen forests was almost always in January, with the POS occurring around August or early September. The EOS for evergreen forests consistently fell in late December,

Table 4
The phenological phase of different crops from 2005 to 2022. The key phenological metrics Start of Season (SOS), Peak of Season (POS) and End of Season (EOS) were calculated based on knowledge-based crop calendars and Savitzky–Golay filter.

Year	BORO			Aman		
	SOS	POS	EOS	SOS	POS	EOS
2005	January	April	June	July	September	December
2006	January	April	June	July	September	December
2007	January	April	June	July	September	December
2008	January	March	June	July	September	December
2009	January	April	June	July	October	December
2010	January	April	June	July	October	December
2011	January	March	June	July	September	December
2012	January	April	June	July	September	December
2013	February	April	June	July	October	December
2014	January	April	June	July	October	December
2015	January	April	June	July	September	November
2016	January	April	June	July	October	November
2017	January	April	June	July	September	November
2018	January	April	June	July	October	December
2019	January	April	June	July	October	November
2020	January	April	June	July	September	December
2021	January	April	June	July	September	December
2022	January	April	June	July	October	December

Table 5
The phenological phase of different forest type from 2005 to 2022. The key phenological metrics Start of Season (SOS), Peak of Season (POS) and End of Season (EOS) were calculated for the deciduous forest based on knowledge based phenological phase and Savitzky–Golay filter using NDVI data. Since evergreen forests remain active throughout the year, only the POS is included for them.

Year	Deciduous Forest			Evergreen Forest
	SOS	POS	EOS	POS
2005	April	August	November	August
2006	April	September	November	September
2007	March	October	November	August
2008	April	September	November	August
2009	March	September	November	September
2010	March	September	November	September
2011	March	September	November	August
2012	March	September	November	September
2013	March	September	November	September
2014	March	October	November	September
2015	March	September	November	September
2016	April	August	November	August
2017	March	October	November	September
2018	March	September	November	September
2019	April	August	November	August
2020	March	September	November	August
2021	April	October	November	August
2022	March	September	November	September

indicating year-round growth, typical of evergreen species (Hussain and Islam, 2020; Khan et al., 2024). These patterns remained relatively stable throughout the study period, suggesting that evergreen forests are less susceptible to short-term climatic variations compared to deciduous forests. The observed variations in SOS, POS, and EOS for both forest types highlight the influence of annual

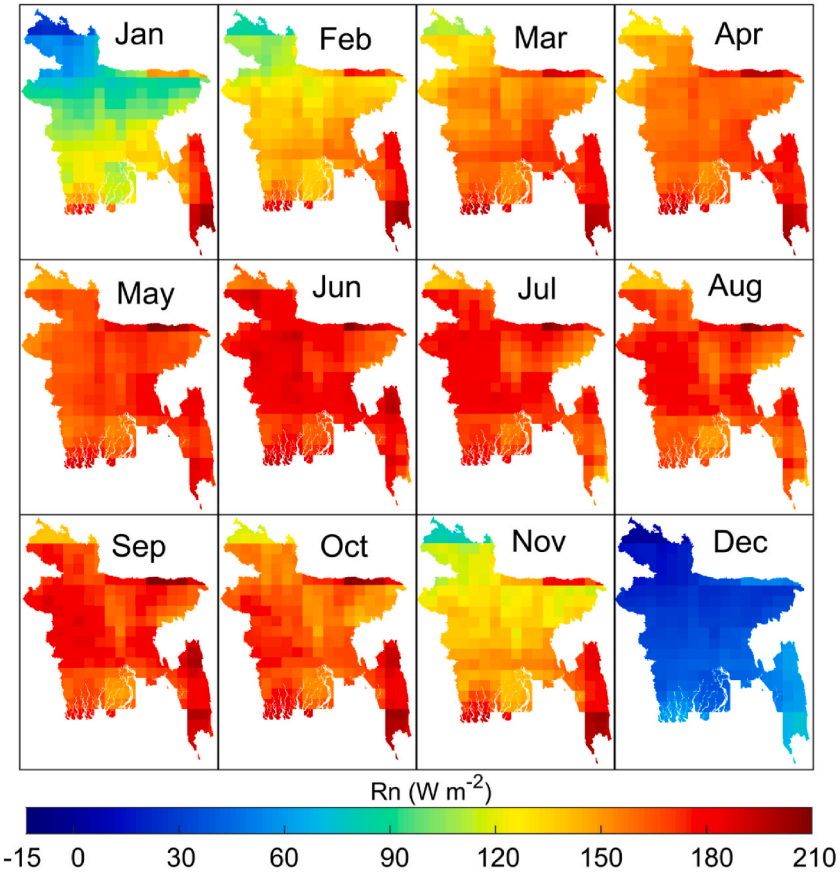

Fig. 5. Spatial distribution of monthly average net radiation (Rn) in W m^{-2} from 2005 to 2022.

climatic conditions on vegetation dynamics. While evergreen forests exhibit a more stable and year-round growth cycle, deciduous forests are more sensitive to seasonal climate fluctuations, leading to notable interannual variability in their phenological phases.

3.2. Energy and water balance

The analysis of energy fluxes from 2005 to 2022 in Bangladesh revealed notable trends in partitioning Rn and LE, with distinct seasonal and annual patterns. Annual Rn decreased from 82.53 W m^{-2} in 2005 to 71.64 W m^{-2} in 2022, with an overall mean of 78.29 W m^{-2}. The highest yearly Rn occurred in 2012 (85.85 W m^{-2}), while the lowest was recorded in 2022 (71.64 W m^{-2}), indicating a reduction over the study period. Monthly Rn data demonstrated significant seasonal variability, with peak values in June (172.39 W m^{-2}) and May (151.86 W m^{-2}), corresponding to the pre-monsoon and monsoon seasons when solar radiation is maximal (Figs. 5 and 6). In contrast, the lowest values were observed in January (−5.60 W m^{-2}) and December (−6.54 W m^{-2}), during winter months when solar radiation is minimal. LE showed similar patterns, ranging from 55.74 W m^{-2} in 2016 to 74.69 W m^{-2} in 2021, with an overall mean of 64.54 W m^{-2}. Monthly LE values peaked in July (133.00 W m^{-2}) and June (116.88 W m^{-2}) during the monsoon season, while the lowest values were observed in January (25.70 W m^{-2}) and December (25.94 W m^{-2}), reflecting the dry winter months. These trends highlight the strong influence of solar radiation and moisture availability on both Rn and LE in Bangladesh.

The LE/Rn ratio analysis from 2005 to 2022 further illuminates the partitioning of net radiation into latent heat flux. The yearly LE/Rn ratio ranged from 0.72 in 2012 and 2016 to 1.02 in 2021 and 2022, with an overall mean of 0.83, indicating that, on average, 83 % of Rn was transferred to the atmosphere as LE. The highest yearly ratios (1.02) occurred in 2021 and 2022, reflecting higher evapotranspiration than net radiation. Conversely, the lowest ratios (0.72) were observed in 2012 and 2016, indicating reduced evapotranspiration. Monthly LE/Rn ratios followed a strong seasonal trend, with the highest values recorded in October (1.09) and November (2.48) during the post-monsoon period, while the lowest values were observed in January (−4.59) and December (−3.97), corresponding to the winter months. These seasonal trends highlight the significant role of evapotranspiration in the energy and water balance of Bangladesh, particularly during the monsoon and post-monsoon months.

H and G showed notable seasonal and annual fluctuations between 2005 and 2022. H values ranged from −1.91 W m^{-2} in 2021 to 23.87 W m^{-2} in 2012, with an overall mean of 13.74 W m^{-2}. The highest yearly H was recorded in 2012 (23.87 W m^{-2}), while the lowest values were in 2021 (−1.91 W m^{-2}) and 2022 (−1.27 W m^{-2}), indicating a shift toward reduced sensible heat flux in recent years. Monthly data showed peak H values in May (57.36 W m^{-2}) and April (48.20 W m^{-2}) during the pre-monsoon months, while the lowest values were recorded in December (−22.67 W m^{-2}) and January (−18.80 W m^{-2}), reflecting surface cooling during winter. Ground heat flux (G) demonstrated near-zero mean values (−0.0008 W m^{-2}), with the highest positive G occurring in 2011 (0.87 W m^{-2}) and the lowest negative value in 2013 (−0.87 W m^{-2}). Monthly G values peaked in April (10.57 W m^{-2}) and May (9.26 W m^{-2}) during the pre-monsoon months, and negative peaks were recorded in December (−9.81 W m^{-2}) and January (−12.51 W m^{-2}), reflecting the influence of solar radiation and temperature on ground heat dynamics.

ET trends from 2005 to 2022 showed a gradual increase, from 1.64 mm in 2005 to 1.79 mm in 2022, with a mean of 1.68 mm. The

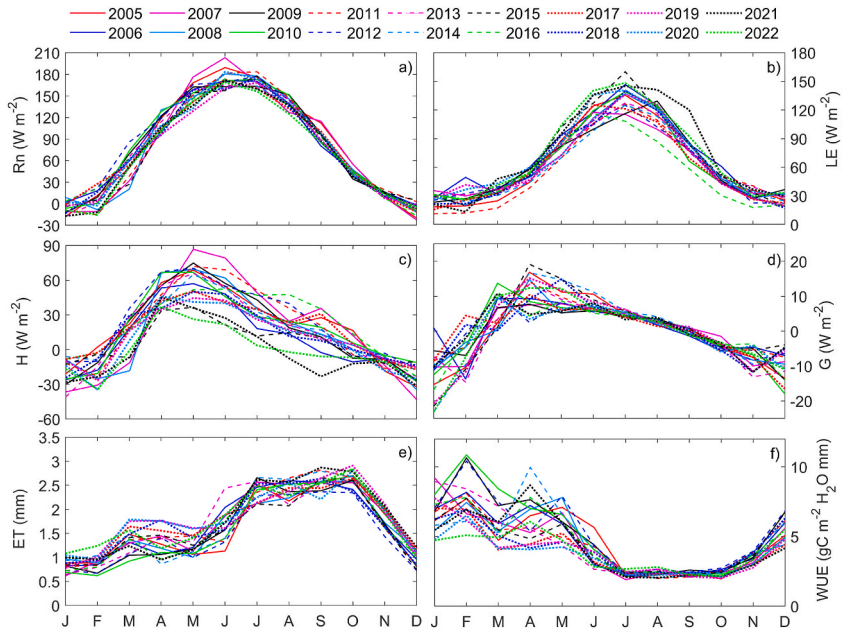

Fig. 6. Monthly energy and water fluxes from 2005 to 2022: a) Net Radiation (Rn) in W m^{-2}, b) Latent heat flux (LE) in W m^{-2}, c) Sensible heat flux (H) in W m^{-2}, d) Ground heat flux (G) in W $m^{-2,}$ e) water dynamics, represented by Evapotranspiration (ET) in mm and f) monthly water use efficiency (WUE) in g C m^{-2} H_2O mm.

highest yearly ET occurred in 2019 (1.82 mm), and the lowest in 2012 (1.47 mm), reflecting active climatic conditions and vegetation activity variability. Monthly ET displayed distinct seasonal patterns, with peak values in October (2.65 mm) and September (2.57 mm), coinciding with the post-monsoon period when moisture availability and vegetation activity were high. During the dry winter months, the lowest values were observed in January (0.84 mm) and February (0.88 mm). This seasonal pattern emphasizes the strong influence of seasonal moisture, solar radiation, and vegetation on ET, with peak values during the monsoon and post-monsoon months (June to November) and a significant reduction in winter (December to February). These trends highlight the interplay between water and energy fluxes, where seasonal variations in solar radiation and moisture availability influence both evapotranspiration and energy balance, shaping the overall climate dynamics of Bangladesh.

3.3. Spatial and temporal distribution of carbon balance

The annual GPP, RE, and NPP variation from 2005 to 2022 reveals significant interannual fluctuations (Figs. 7 and 8). The daily mean GPP was 6.25 ± 0.89 g C m^{-2} d^{-1}, with the highest recorded in 2009 (6.44 g C m^{-2} d^{-1}) and the lowest in 2020 (5.97 g C m^{-2} d^{-1}). RE exhibited an overall mean of 3.39 ± 1.11 g C m^{-2} d^{-1}, with values ranging from 3.07 g C m^{-2} d^{-1} in 2012 to 3.71 g C m^{-2} d^{-1} in 2019. Annual NPP averaged 3.02 ± 1.31 g C m^{-2} d^{-1}, with the highest value in 2012 (3.42 g C m^{-2} d^{-1}) and the lowest in 2020 (2.55 g C m^{-2} d^{-1}). Correlation between observed GPP (from FLUXCOM) and measured GPP (from the LUE model) shows a strong positive relationship with an R^2 of 0.61, meaning 61 % of the GPP variability is explained by the observed data (Fig. 3b). The correlation was statistically significant ($p < 0.005$), confirming the LUE model's reliability in estimating GPP. A combination of climatic conditions, land management practices, and ecosystem responses to environmental stresses drives these variations. The significantly lower NPP in 2020 likely reflects the impacts of extreme climatic events, which disrupted vegetation productivity.

The long-term seasonal analysis of carbon fluxes (2005–2022) further underscores observed fluctuations in GPP (Fig. 10), RE, and NPP across the year. GPP peaked in September (361 ± 9 g C m^{-2} mo^{-1}) and October (357 ± 12 g C m^{-2} mo^{-1}), while the lowest values occurred in December (86 ± 3 g C m^{-2} mo^{-1}) and January (95 ± 4 g C m^{-2} mo^{-1}). RE followed a clear seasonal pattern, with peaks in February (152 ± 2 g C m^{-2} mo^{-1}) and January (143 ± 4 g C m^{-2} mo^{-1}), and the lowest values observed in May (48 ± 2 g C m^{-2} mo^{-1}). NPP was highest in May (140 ± 4 g C m^{-2} mo^{-1}) and followed by October (134 ± 5 g C m^{-2} mo^{-1}) September (130 ± 5 g C m^{-2} mo^{-1}) and April (130 ± 2 g C m^{-2} mo^{-1}), while loest C uptake was in December and January almost the Carbon Neutral (~12–20 g C m^{-2} mo^{-1}). The highest GPP and NPP during March–April reflects the peak growing season of winter crops, while the September–October period marks the dominance of monsoon crop carbon uptake, aligning with the second phase of the crop calendar. These trends highlight key phenological metrics of the ecosystem (Tables 4 and 5). The decline in biomass productivity and carbon uptake in December–January corresponds with winter climatic conditions, characterized by reduced solar radiation and increased soil moisture,

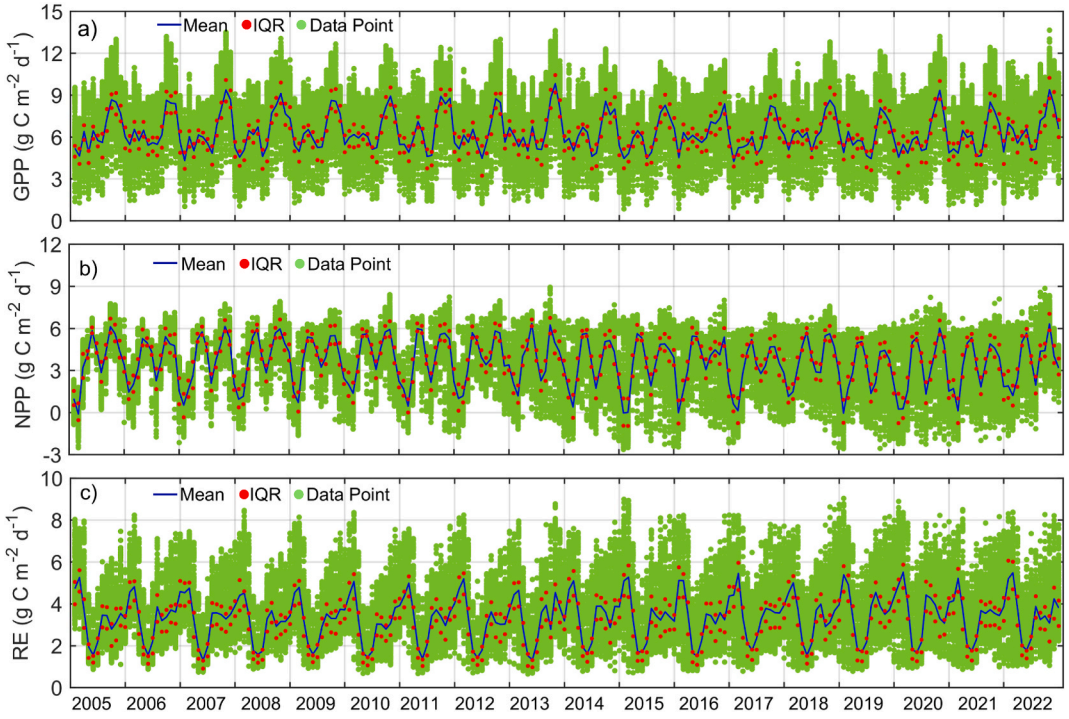

Fig. 7. Monthly carbon balance time series from 2005 to 2022, showing daily GPP (a), NPP (b), and RE (c) expressed in g C m^{-2} d^{-1}. In each panel, the blue solid line represents the monthly mean, green dots indicate individual daily observations, and red dots mark the interquartile range (IQR = Q3 − Q1) for each month, illustrating variability in ecosystem carbon fluxes.

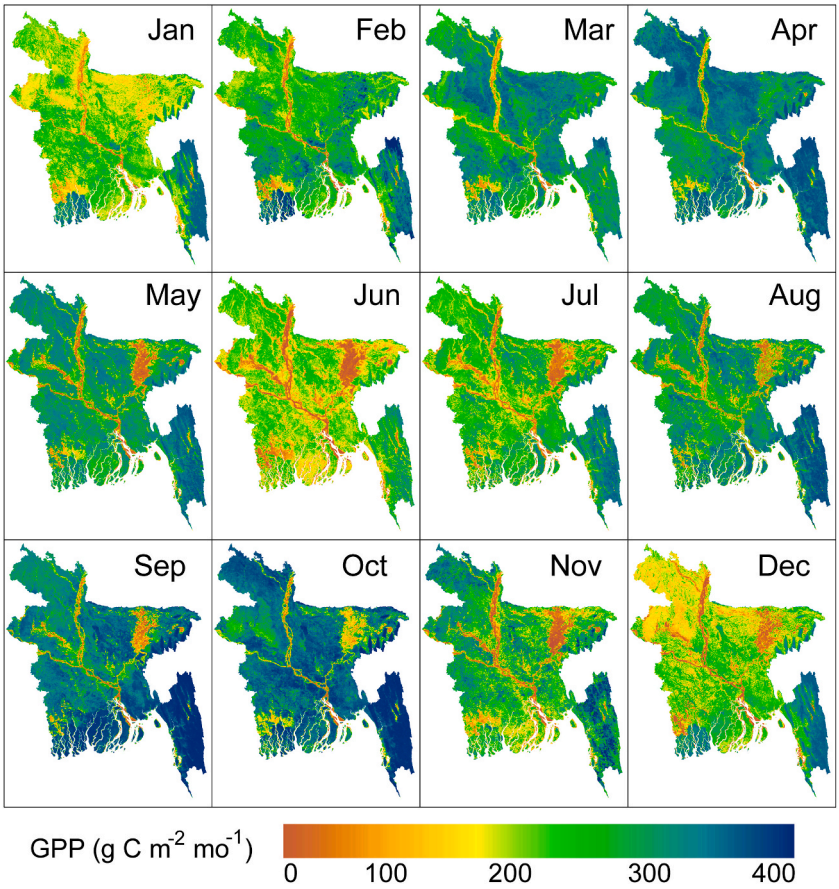

Fig. 8. Spatial distribution of monthly average Gross Primary Production (GPP) in g C m-^{2} mo^{-1} from 2005 to 2022.

Table 6
Yearly comparison of biomass, water, energy and carbon balance parameters, including daily LAI leaf area index (LAI in m^2/m^2; daily ET in mm, yearly total Gross Primary Production (GPP), yearly total Ecosystem Respiration (RE), yearly total Net Primary Production (NPP), total carbon uptake from country in ($MtCO_2e$), net carbon uptake ($MtCO_2e$), and carbon emissions for the years 2005–2022. The values are presented with their respective standard deviations where applicable. The total CO_2 emissions data for Bangladesh is sourced from the Ministry of Environment, Forest, and Climate Change, Bangladesh, for 2019 (DoE, 2023), and from the CO_2 and GHG Emission Reports by the European Commission for the years 2020–2023 (Crippa et al., 2024).

Year	LAI (m^2/m^2)	ET (mm d^{-1})	GPP ($gCm^{-2}y^{-1}$)	RE ($gCm^{-2}y^{-1}$)	NPP ($gCm^{-2}y^{-1}$)	Total Uptake ($MtCO_2e$)	Net-Uptake ($MtCO_2e$)	Emission ($MtCO_2e$)
2005	1.28 ± 0.37	1.64 ± 0.69	2304.32	1167.85	1189.61	1253.60	647.17	39.77[a]
2006	1.33 ± 0.37	1.66 ± 0.71	2337.17	1239.60	1144.87	1271.47	622.84	42.76[a]
2007	1.25 ± 0.31	1.70 ± 0.73	2271.01	1200.96	1133.75	1235.48	616.79	45.20[a]
2008	1.25 ± 0.39	1.64 ± 0.63	2287.81	1164.91	1180.07	1244.63	641.99	50.54[a]
2009	1.27 ± 0.38	1.57 ± 0.75	2351.29	1184.02	1218.90	1279.16	663.11	53.73[a]
2010	1.23 ± 0.35	1.59 ± 0.79	2319.39	1144.30	1230.46	1261.81	669.40	59.55[a]
2011	1.32 ± 0.41	1.68 ± 0.75	2292.70	1216.84	1130.96	1247.28	615.27	63.40[a]
2012	1.29 ± 0.38	1.47 ± 0.68	2300.69	1119.83	1248.13	1251.63	679.01	169.05
2013	1.36 ± 0.45	1.72 ± 0.74	2285.27	1252.11	1091.70	1243.24	593.91	174.62
2014	1.40 ± 0.45	1.67 ± 0.79	2325.69	1278.10	1104.49	1265.23	600.87	179.26
2015	1.41 ± 0.44	1.60 ± 0.65	2223.06	1231.47	1043.32	1209.39	567.59	187.98
2016	1.43 ± 0.39	1.64 ± 0.75	2267.22	1244.95	1078.77	1233.42	586.88	196.79
2017	1.46 ± 0.41	1.76 ± 0.59	2208.63	1274.89	984.38	1201.55	535.52	198.1
2018	1.47 ± 0.49	1.72 ± 0.66	2279.02	1258.43	1078.12	1239.84	586.52	206.87
2019	1.57 ± 0.47	1.82 ± 0.66	2285.74	1354.82	980.72	1243.49	533.53	213.19
2020	1.46 ± 0.39	1.81 ± 0.59	2178.45	1303.33	929.46	1185.13	505.65	269.03
2021	1.47 ± 0.47	1.76 ± 0.77	2256.77	1324.40	991.63	1227.73	539.47	276.8
2022	1.49 ± 0.41	1.79 ± 0.64	2280.11	1301.26	1049.43	1240.44	570.92	278.49

[a] Note: The total emission only includes industrial and fuel burn emissions, collected from Our World in Data (Ritchie et al., 2020).

as well as the transitional periods between the two main cropping systems. Similarly, the reduction observed in June and July is influenced by heavy monsoon rainfall, major shifts in the crop season, and flooding of lowland areas, which limit terrestrial carbon uptake. However, riparian vegetation remains active in this period to biomass production, continuing its role in the ecosystem until August (Fig. 8).

Climatic drivers notably shape the seasonal variability in carbon fluxes. The pre-monsoon period (March–May) is marked by favorable conditions for growth, with higher GPP and NPP driven by increased solar radiation and moderate soil moisture. In contrast, the monsoon season (June–July) reduces GPP and NPP, likely due to waterlogged soils, diminished sunlight, and increased respiration losses. During the post-monsoon and winter months (October–November), GPP and NPP increase, while RE remains relatively lower, supporting carbon sequestration. The peak RE observed in September and October suggests a delayed response in microbial decomposition, driven by warm and moist conditions, which accelerate microbial activity. These seasonal dynamics are intricately linked to temperature, precipitation patterns, and the growing season, which determine the net carbon balance in terrestrial ecosystems.

From 2005 to 2022, the carbon balance exhibited notable fluctuations. GPP ranged from 2178.45 g C m^{-2} y^{-1} in 2020–2351.29 g C m^{-2} y^{-1} in 2009, reflecting the variation in photosynthetic efficiency and carbon capture (Table 6). RE varied from 1119.83 g C m^{-2} y^{-1} in 2012 to 1354.82 g C m^{-2} y^{-1} in 2019, signifying the carbon released back to the atmosphere through plant and soil processes. NPP, the difference between GPP and RE, exhibited significant fluctuation, with the lowest in 2020 (929.46 g C m^{-2} y^{-1}) and the highest in 2012 (1248.13 g C m^{-2} y^{-1}), underscoring variability in carbon storage within plant biomass.

Over the study period, total carbon uptake slightly decreased, from 1253.60 $MtCO_2e$ in 2005 to 1240.44 $MtCO_2e$ in 2022, with a peak of 1279.16 $MtCO_2e$ in 2009 (Table 6). Conversely, emissions followed a consistent upward trend, rising from 39.77 $MtCO_2e$ in 2005 to 281.08 $MtCO_2e$ in 2022, with the largest increases observed post-2012. This widening gap between carbon uptake and carbon emissions highlights the growing disparity between the carbon sequestration capacity of ecosystems and the emissions resulting from human activities, such as deforestation and land-use changes. This trend signals an increasing challenge in mitigating the adverse impacts of climate change, underscoring the need for urgent action to curb emissions and enhance carbon capture in natural systems.

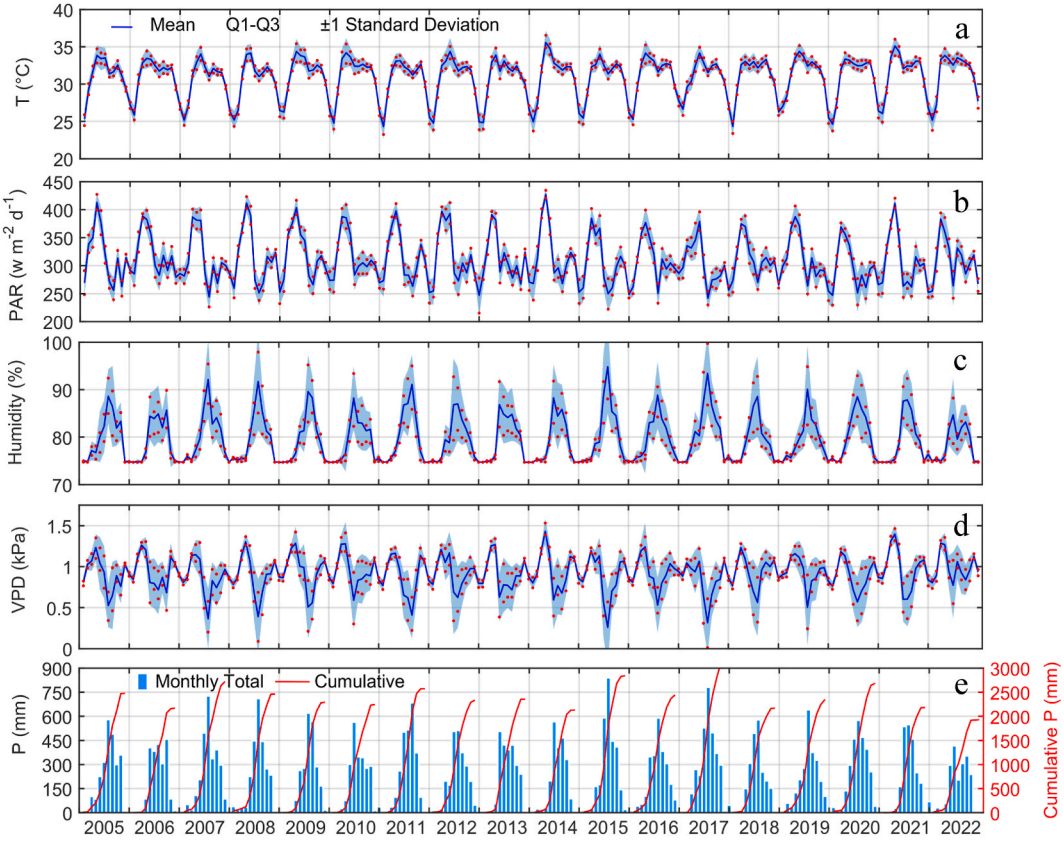

Fig. 9. Climatic variables from 2005 to 2022. The dark blue line represents the monthly average, while the shaded area indicates the mean ± 1 standard deviation and the red dot shows the interquartile range (IQR = Q3 − Q1) for each month in panels a–d, a) Monthly average temperature (T) in °C, b) Monthly average Photosynthetically Active Radiation (PAR) in W m^{-2}, c) Monthly Normal Humidity (%), d) Monthly Vapor Pressure Deficit (VPD) in kPa, and (e) Monthly total Precipitation (P) in mm with the blue bar with the red line representing the yearly cumulative P.

3.4. Climatic drivers on water, energy, and carbon balance

The variability in biomass productivity and phenology in Bangladesh is strongly influenced by seasonal patterns and prevailing climatic conditions. From 2005 to 2022, yearly average temperatures ranged from 30.44 ± 2.75 °C in 2007 to 31.54 ± 2.87 °C in 2021, with an overall mean of 30.98 ± 2.82 °C, while monthly temperatures followed a clear seasonal cycle, peaking in May (33.66 ± 0.75 °C) and lowest in January (25.34 ± 0.76 °C), with the highest standard deviation in February (1.08 °C) and lowest in September (0.41 °C), reflecting greater variability during transitional months (Fig. 9a). Similarly, yearly average photosynthetically active radiation (PAR) fluctuated between 297.55 ± 39.88 W m^{-2} in 2020 and 321.14 ± 45.23 W m^{-2} in 2009, with an overall mean of 311.57 ± 44.28 W m^{-2}, while monthly PAR peaked in April (384.74 ± 22.75 W m^{-2}) and May (374.99 ± 16.54 W m^{-2}) and reached minima in December (271.75 ± 14.26 W m^{-2}) and January (286.68 ± 11.16 W m^{-2}) (Fig. 9b).

Annual precipitation showed considerable variability, with the highest total in 2017 (3160.28 mm) and lowest in 2022 (1928.84 mm), and a long-term average of ~2500 mm, while monthly precipitation peaked during the monsoon in July (555.08 mm), June (452.06 mm), and May (266.18 mm) and reached minima in the dry season in January (7.56 mm), February (16.59 mm), and December (10.75 mm) (Fig. 9e). Monthly humidity increased from 74.88 % in January to 85.55 % in June, then declined to 74.96 % by December, reflecting higher moisture during the monsoon and lower during winter (Fig. 9c). Likewise, monthly vapor pressure deficit (VPD) ranged from 0.60 kPa in July to 1.20 kPa in April, with higher values during dry months and lower values during the humid monsoon, indicating strong seasonal variability in atmospheric moisture that influences hydrological and ecosystem processes (Fig. 9d).

The annual WUE from 2005 to 2022 exhibited significant interannual variability, with values ranging from 3.67 ± 1.36 (g C m^{-2} H_2O mm) in 2020 to 5.29 ± 2.63 (g C m^{-2} H_2O mm) in 2012, and an overall mean of 4.50 ± 2.12 (g C m^{-2} H_2O mm). Peak WUE values were observed in 2009 and 2010, reaching 5.20 (g C m^{-2} H_2O mm), while the lowest value occurred in 2020. Monthly analysis revealed a clear seasonal pattern, with the highest WUE in February (7.70 ± 1.59 g C m^{-2} H_2O mm) and January (6.70 ± 1.26 g C m^{-2} H_2O mm) and the lowest in July (2.28 ± 0.18 g C m^{-2} H_2O mm) and September (2.30 ± 0.14 g C m^{-2} H_2O mm). This variation is closely tied to crop growth cycles, water availability, and climatic conditions, with higher WUE during the dry winter and early growing season months and lower WUE during the monsoon period due to increased evapotranspiration and precipitation. The WUE trends highlight the influence of crop type, soil moisture, and meteorological factors on the carbon-water relationship within Bangladesh's agricultural ecosystems. This pattern is further reflected in the overall carbon balance, where the interplay between water availability and carbon fluxes underlines the sensitivity of agricultural productivity and carbon sequestration to climatic shifts.

The relationship between carbon and water balance is illustrated by the association of GPP and ET (Fig. 10a) demonstrates a strong positive coupling between carbon assimilation and water loss across the study ecosystem ($R^2 = 0.42$, $P < 0.005$). The peak data density occurs at GPP ≈ 6–8 g C m^{-2} d^{-1} and ET ≈ 1.5–2.0 mm d^{-1}, reflecting the dominant operating range of the ecosystem. The slope of the regression line suggests an average ecosystem WUE of approximately 3–4 g C kg^{-1} H_2O (derived from the ratio of GPP to ET), which is consistent with well-watered crop and grassland systems. Occasional high-ET points with moderate GPP indicate periods of lower WUE, likely driven by evaporative water loss under high VPD conditions or following irrigation events. The clear coupling between GPP and ET highlights the ecosystem's strong carbon–water linkage, where enhanced photosynthesis generally coincides with higher transpiration.

The relationship between GPP, representing the ecosystem carbon balance and PAR, the driving light energy, exhibits the classical light-response curve, with GPP increasing sharply at low PAR before reaching saturation beyond ~350 W m^{-2} (Fig. 10b). Bin-averaged GPP values indicate that GPP rises from near 0–~10 g C m^{-2} d^{-1} as PAR increases from 0 to 500 W m^{-2}, with the hyperbolic fit (Fig. 10b, black line) showing a clear asymptotic trend. The initial slope of the curve, representing ecosystem light-use efficiency, is

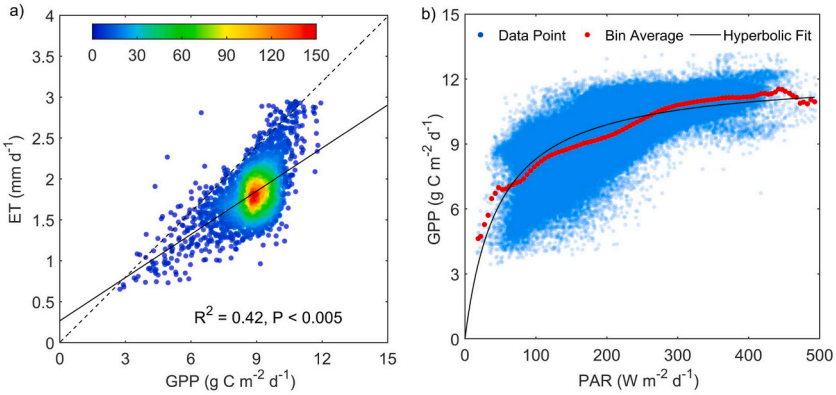

Fig. 10. (a) Relationship between gross primary productivity (GPP) and evapotranspiration (ET). Point density is shown by the color map, with warmer colors indicating higher data density. The strong positive relationship highlights coupled carbon–water dynamics, where higher GPP is generally associated with increased ET. (b) Relationship between GPP and photosynthetically active radiation (PAR). Individual observations (blue) display the typical light-response pattern. Red points represent GPP values averaged within 10s (W m^{-2}) PAR bins, while the black line shows the fitted hyperbolic curve, illustrating the hyperbolic curve fit to highlight the optimal photosynthetic capacity.

highest under low light conditions, implying that the ecosystem efficiently converts absorbed light to carbon when radiation is limiting. At higher PAR, GPP approaches saturation (~10–11 g C m^{-2} d^{-1}), suggesting biochemical or stomatal constraints on photosynthesis rather than light limitation. This pattern aligns with the light-response behaviors of productive croplands, where LUE declines as other factors (e.g., water or nutrient availability) become limited at high irradiance levels.

The MLR analysis was performed to quantify the relationship among climatic variables and carbon-water-energy fluxes (Table 7). GPP, representing the carbon balance was strongly controlled by light energy PAR exhibited the strongest positive relationship, explaining the majority of the variance ($R^2 = 0.97$), while temperature and radiative energy Rn had a much smaller influence, with R^2 values of 0.29 and 0.03, respectively. In contrast, NPP was most strongly influenced by precipitation ($R^2 = 0.37$), followed by PAR ($R^2 = 0.28$) with minor contribution from Rn ($R^2 = 0.08$). RE was largely driven by temperature emerged as the most significant driver, accounting for 57 % of the variance ($R^2 = 0.57$), followed by precipitation ($R^2 = 0.21$). Meanwhile, ET, representing the water balance, showed the highest association with water availability ($R^2 = 0.37$), with temperature playing a secondary role ($R^2 = 0.24$). Overall, the MLR results confirm that light availability and temperature are the dominant factors controlling carbon uptake and respiration, while precipitation and net radiation exhibit more variable effects on NPP and RE. The results also present the mechanistic coupling among carbon uptake, respiration, and water fluxes, reflecting their shared dependencies on light, temperature, and moisture, although part of the coherence may result from the use of common input datasets in the modeling framework.

4. Discussion

4.1. The climatic conditions and vegetation dynamics

The climatic conditions and vegetation dynamics in Bangladesh from 2005 to 2022 exhibit distinct seasonal patterns closely linked to the country's agroecological environment. The stable annual temperature range (30.44 ± 2.75 °C to 31.54 ± 2.87 °C) aligns with the tropical monsoon climate, where the warmest months (April–June) coincide with the pre-monsoon growing season, while cooler months (November–January) mark the dry season, influencing crop cycles and water demand (Rahman and Anik, 2020). The observed variations in PAR, which peak in March–April and decline in January, play a crucial role in determining photosynthetic efficiency and crop productivity, particularly for rice, the dominant staple crop (Acevedo-Siaca et al., 2020; Al Mamun et al., 2025). Precipitation trends, with the highest annual total recorded in 2017 (3160.28 mm) and the lowest in 2022 (1928.84 mm), underscore the strong monsoonal influence. The peak rainfall from July to August dictates water availability for rain-fed agriculture and the succession of major cropping seasons (Aus and Aman rice) (Rahman et al., 2017; Saini et al., 2020).

The seasonal trends in NDVI (0.49 in 2005 to 0.55 in 2022) and LAI (1.28 m^2/m^2 in 2005 to 1.49 m^2/m^2 in 2022) reflect the

Table 7
Results of Multiple Regression Analysis (MLR) quantifying the relationship between climatic variables and carbon fluxes. The analysis includes the relationship between temperature, precipitation, photosynthetically active radiation (PAR), and net radiation (Rn) with Gross Primary Production (GPP), Net Primary Production (NPP), and Respiration (RE). R^2 values are provided for each variable's contribution to explaining the variance in the respective carbon fluxes. The significance level is indicated based on the P value, where * represents non-significance ($P \geq 0.05$), ** shows weak to moderate significance ($P \leq, \approx 0.05$) and *** indicates very strong significance ($p \leq 0.001$).

GPP						
Variable	Intercept	Slope	Standard Error	R^2	RMSE	Significance
Temperature	0.98	0.17	0.73	0.29	0.53	**
Precipitation	6.55	0.001	0.81	0.13	0.66	**
PAR	0.01	0.001	0.01	0.97	0.01	***
Rn	5.79	0.14	0.85	0.03	0.73	*
NPP						
Variable	Intercept	Slope	Standard Error	R^2	RMSE	Significance
Temperature	6.78	−0.102	1.2	0.07	1.45	**
Precipitation	3.77	0.001	0.99	0.37	0.98	**
PAR	−1.76	0.001	1.06	0.28	1.12	***
Rn	3.43	−0.001	1.19	0.08	1.43	*
RE						
Variable	Intercept	Slope	Standard Error	R^2	RMSE	Significance
Temperature	−5.87	0.3	0.71	0.57	0.51	***
Precipitation	2.9	0.001	0.96	0.21	0.93	*
PAR	1.99	0.001	1.06	0.03	1.14	*
Rn	2.81	0.001	0.96	0.21	0.91	**
ET						
Variable	Intercept	Slope	Standard Error	R^2	RMSE	Significance
Temperature	−2.07	0.12	0.59	0.24	0.35	***
Precipitation	1.27	0.001	0.54	0.37	0.29	***
PAR	2.91	0.001	0.66	0.06	0.43	**
Rn	1.35	0.001	0.62	0.17	0.38	*

influence of climatic variability on biomass production, with peak vegetation health observed in the post-monsoon period (September–October). This period supports Aman rice and late summer vegetable cultivation and forest regrowth. In contrast, the lowest NDVI and LAI values during the monsoon season (May to September) suggest temporary reductions in vegetation indices due to cloud cover and waterlogging, which negatively impact agricultural productivity and forest ecosystems. These findings highlight the intricate linkages between Bangladesh's seasonal climate variability, agroecosystem dynamics, and vegetation productivity, emphasizing the importance of adaptive land and water management strategies to sustain agricultural resilience under changing climatic conditions (Rahman and Anik, 2020; Bhatnagar et al., 2024).

4.2. Remote sensing-based carbon water and energy dynamics

The spatiotemporal analysis of energy, water, and carbon fluxes in Bangladesh from 2005 to 2022 reveals significant seasonal and interannual variability. Net radiation (Rn) declined from 82.53 W m^{-2} in 2005 to 71.64 W m^{-2} in 2022, likely due to increased cloud cover and atmospheric changes that reduced solar radiation. LE, the dominant component of energy partitioning, exhibited an increasing trend in recent years, with a mean value of 64.54 W m^{-2}, highlighting the crucial role of evapotranspiration in energy dissipation. Seasonal fluctuations were evident, with peak LE values observed during the monsoon months (May to September) and lower values during winter (December–January), reflecting the influence of solar radiation and moisture availability (Dastour et al., 2025). The LE/Rn ratio, averaging 0.83, highlights the predominance of latent heat flux in the energy balance, particularly during the post-monsoon season, when excess energy is directed toward evapotranspiration. These findings align with previous studies emphasizing the role of monsoon-driven hydro-climatic processes in shaping Bangladesh's energy and water cycles (Jihan et al., 2025).

Carbon flux trends indicate that climate variability and land-use changes significantly influence Bangladesh's carbon balance. The mean annual GPP of 6.25 ± 0.89 g C m^{-2} d^{-1}, with two peaks in September–October and April, emphasizes the dependency of carbon assimilation on solar radiation and temperature and is highly influenced by crop cultivation. The sharp decline in NPP in 2020, likely driven by extreme climatic events such as prolonged droughts in winter and the floods in monsoon, highlights the vulnerability of carbon sequestration to climate anomalies. Additionally, carbon emissions increased substantially from 39.77 $MtCO_2$ in 2005 to 281.08 $MtCO_2$ in 2022, suggesting that anthropogenic influences, including deforestation, urbanization, and land-use conversion, are outpacing the natural carbon sink capacity (Majumder et al., 2019; Tadese et al., 2023). The rising trends in emissions, coupled with the declining carbon uptake, underscore the urgent need for climate mitigation strategies such as afforestation, improved land management practices, and targeted emission reduction policies, particularly in monsoon-dominated ecosystems (Ayers and Huq, 2009; Lee et al., 2024).

The agricultural ecosystem plays a dominant role in shaping the carbon balance of the study area, influencing both carbon uptake and emissions (Hussain et al., 2021). Under natural climatic conditions, winter would typically contribute less to carbon sequestration due to lower temperatures, reduced solar energy, and limited water availability. However, the extensive and widespread irrigation practice has significantly altered this seasonal dynamic, enabling winter crops to continue absorbing carbon despite these constraints. This adaptation not only supports agricultural productivity but also provides ecosystem benefits by maintaining carbon assimilation during a season that would otherwise see a decline. However, while total carbon assimilation remains relatively stable, net carbon uptake is decreasing due to factors such as increased soil respiration, fertilizer application, and emissions from agricultural activities. The role of agriculture in carbon cycling extends beyond crop growth—it encompasses land-use decisions, farming techniques, and economic policies that collectively shape the movement and storage of carbon within the system. By integrating ecological processes with socioeconomic considerations, policymakers can develop strategies that mitigate emissions and enhance carbon sequestration, ensuring a sustainable future for both agriculture and the broader ecosystem (Jihan et al., 2025).

The interactions between energy, water, and carbon fluxes are closely linked to seasonal monsoon patterns and long-term climate trends. The positive correlation between LE and GPP suggests that higher evapotranspiration during monsoon months supports greater carbon uptake, reinforcing the crucial role of water availability in ecosystem productivity. The observed NPP peak during the pre-monsoon season corresponds with optimal solar radiation conditions, indicating a strong dependence of carbon assimilation on energy fluxes. However, in post-monsoon and winter months, carbon uptake decreases due to reduced photosynthetic activity and lower water availability. These findings signify the regional studies emphasizing the coupling of hydrological and carbon cycles in monsoon-driven ecosystems. The results underscore the need for integrated climate resilience strategies that consider the interconnected nature of energy, water, and carbon dynamics to sustain ecosystem services and mitigate climate change impacts in Bangladesh (Hussain et al., 2021; Jihan et al., 2025).

This study recognizes key uncertainties arising from satellite-derived inputs (NDVI, LAI, PAR, LST), meteorological observations in dynamic tropical region, and model assumptions. Variability in spatial resolution, temporal coverage, and measurement techniques contributes to differences in modeled GPP (Deng et al., 2019; Guan et al., 2021; Yang et al., 2021; Hussain et al., 2024b; Wang et al., 2024; Isik et al., 2025). While modeled GPP showed strong agreement with FLUXCOM and GOSIF datasets ($R = 0.58–0.61$, $P < 0.0001$), light saturation at ~10–11 g C m^{-2} d^{-1} also indicates physiological limitations under high solar radiation levels (Fig. 10b). These uncertainties highlight the need for cautious interpretation of carbon fluxes and emphasize the value of LUE-based models in capturing carbon–water–energy dynamics in monsoon-influenced ecosystems, guiding future improvements in remote sensing and process-based modeling frameworks (Ma et al., 2025; Yuan et al., 2025).

4.3. Controlling factors of water, energy, and carbon balance

The relationship between climatic drivers and the water, energy, and carbon fluxes in Bangladesh's agricultural ecosystems was

explored using MLR (Table 7). The MLR indicated that PAR had the strongest relationship with GPP ($R^2 = 0.97$), while temperature and Rn had more modest effects. For NPP, precipitation emerged as the dominant driver, explaining 37 % of the variance, whereas temperature and PAR had weaker correlations. Regardless of RE, temperature was the most significant variable, explaining 57 % of the variance, followed by precipitation.

The WUE analysis from 2005 to 2022 revealed substantial interannual and seasonal variability. Peak WUE values were observed in 2009 and 2010, whereas the lowest values occurred in 2020. The highest WUE values were recorded during the dry winter months, with February and January showing the most efficient use of water during the period of limited precipitation. Conversely, the lowest WUE values were observed in the monsoon months of July and September, likely due to increased evapotranspiration and precipitation (Rahman et al., 2017; Rahman and Anik, 2020). These trends underscore the influence of crop growth cycles and climatic conditions on the carbon-water relationship within agricultural ecosystems, highlighting the sensitivity of carbon sequestration and water use to seasonal and interannual climate fluctuations (Sauer et al., 2007; Hussain et al., 2021).

This study comprehensively assesses of the climatic drivers influencing water, energy, and carbon fluxes in Bangladesh's agricultural ecosystems, utilizing MLR to uncover intricate relationships between climate variables and ecosystem processes. The findings highlight that temperature and PAR are the primary drivers of carbon dynamics, particularly GPP and RE, while precipitation and Rn play secondary roles. Seasonal and interannual variations in WUE further emphasize the sensitivity of agricultural productivity and carbon sequestration to climatic fluctuations, with higher WUE values during dry seasons and lower values during monsoon months. These perceptions emphasize the importance of adaptive agricultural practices to optimize water use efficiency and carbon sequestration, especially in the context of climate change (Islam and Nursey-Bray, 2017).

However, the land-cover changes, including deforestation, urbanization, and cropland expansion over the past 18 years, can substantially shape carbon ecosystem, water, and energy fluxes in the study region (Zhu et al., 2022; Pereira et al., 2024). These transitions influence surface roughness, albedo, soil moisture availability, and vegetation structure, creating additional variability in flux patterns alongside climatic drivers. Considering high-resolution land-cover datasets together with long-term eddy covariance observations will enhance the ability to capture these combined effects and provide a more complete understanding of ecosystem responses to environmental change. The significance of this study lies in its potential to inform adaptive agricultural practices and land management strategies aimed at enhancing carbon sequestration, optimizing water use efficiency, and mitigating climate change impacts in Bangladesh's unique monsoon-dominated ecosystems.

4.4. Study limitations and future directions

This study investigates long-term carbon, water, and energy fluxes in Bangladesh's agricultural ecosystems by integrating multi-source remote sensing data with climate observations from weather stations to identify key climatic drivers. Limitations include the spatially restricted availability of EC flux measurements, constrained by financial and maintenance challenges, as well as seasonal variability in satellite data that may affect the precision of remotely sensed estimates of GPP and carbon uptake (Pei et al., 2022; Sun et al., 2023; Celis et al., 2024; Wang et al., 2024; Wei et al., 2025). Uncertainty is further compounded by seasonal variability in satellite-derived inputs, including NDVI, LAI, PAR, and LST. Persistent cloud cover during the monsoon season (July–September) degrades data quality, resulting in temporal gaps and potential underestimation of fluxes despite the application of compositing and gap-filling techniques. Model-related uncertainty associated with LUE assumptions also influences GPP estimates (Pei et al., 2022; Celis et al., 2024). Specifically, GPP increases rapidly under low PAR conditions but reaches saturation at approximately 10–11 g C m^{-2} d^{-1} when radiation exceeds ~350 W m^{-2}, reflecting physiological constraints and heightened sensitivity to water and nutrient limitations under high radiation regimes.

The coupled carbon–water relationship introduces additional variability. Although GPP and ET exhibit a statistically significant positive relationship ($R^2 = 0.42$, $P < 0.005$), observations are concentrated within moderate ranges of GPP (6–8 g C m^{-2} d^{-1}) and ET (1.5–2.0 mm d^{-1}), corresponding to an average water-use efficiency of approximately 3–4 g C kg^{-1} H_2O (Rotenberg et al., 2025; Hussain et al., 2026). Deviations from this relationship, particularly periods of elevated ET relative to GPP driven by high vapor pressure deficits or irrigation practices, remain difficult to resolve without more spatially extensive EC observations (Celis et al., 2021; Hussain et al., 2024b).

Despite these limitations, the remote sensing–based framework demonstrates strong agreement with independent products, showing significant correlations with FLUXCOM-GPP ($R^2 = 0.61$, $P < 0.005$) and GOSIF-GPP ($R^2 = 0.58$, $P < 0.005$), aligning with previous studies (Hussain et al., 2026). These results indicate that the methodology reliably captures broad-scale patterns of carbon uptake and ecosystem productivity. However, uncertainty increases at regional and ecosystem-specific scales, emphasizing the need for expanded EC networks, improved integration of ground observations with high-resolution satellite data, and explicit uncertainty analyses to enhance future assessments of water, energy, and carbon balances in Bangladesh's monsoon-dominated agricultural systems. Future research integrating land-use dynamics with climate-driven models will support the development of adaptive agricultural strategies, sustainable water management, and improved carbon sequestration planning.

5. Conclusion

This study provides a comprehensive assessment of long-term carbon, water, and energy fluxes in Bangladesh, using multi-source remote sensing data and ground-based climate records from 2005 to 2022. The findings emphasize the significant influence of temperature, PAR, precipitation, and net radiation on carbon, water, and energy fluxes, with temperature and PAR emerging as the dominant drivers of carbon uptake. Temperature plays a crucial role in RE, while precipitation and Rn exerted secondary effects on

carbon uptake, reinforcing the importance of solar radiation and temperature in regulating carbon dynamics. The WUE analysis revealed strong seasonal and interannual variability, with higher values observed in the dry season and lower values during the monsoon. This variability underscores the sensitivity of agricultural productivity and carbon sequestration to climatic fluctuations. Additionally, the energy balance assessment indicated that a significant portion of radiative energy was transferred as LE, particularly during the monsoon and post-monsoon periods, emphasizing the critical role of evapotranspiration in regional climate regulation. Overall, the results emphasize the crucial role of climatic variables, particularly solar radiation, temperature, and precipitation, in driving the energy, water, and carbon fluxes in Bangladesh's agricultural ecosystems.

The study presents the necessity of adapting agricultural practices to enhance water use efficiency and carbon sequestration in response to climate variability. Although uncertainties remain due to seasonal variability in satellite data, persistent monsoon cloud cover and input parameter choices in the LUE model, the analysis of GPP, NPP, and ecosystem respiration reveals clear seasonal patterns in photosynthetic activity and carbon storage. The strong agreement between the estimated GPP and independent products such as FLUXCOM-GPP and GOSIF-GPP confirms the reliability of the modeling framework for national-scale assessments. Despite data and model uncertainties, the results provide reliable and valuable understanding into ecosystem functioning in monsoon-dominated environments.

This study represents a significant advancement in understanding the carbon, water, and energy balance in Bangladesh, marking one of the first comprehensive efforts to assess these crucial fluxes at a national scale. By combining long-term data from remote sensing and ground-based observations, it provides essential insights into the dynamics of agricultural ecosystems under the influence of climate variability. The findings not only inform sustainable land management, water use efficiency, and carbon sequestration strategies but also lay the groundwork for future national-level climate resilience and ecosystem management efforts. These methods and results are particularly valuable for regions with similar climatic conditions, offering a framework to address climate change challenges and enhance agricultural and ecological stability.

CRediT authorship contribution statement

Nur Hussain: Writing – review & editing, Writing – original draft, Visualization, Validation, Methodology, Formal analysis, Conceptualization. **Md Saifuzzaman:** Writing – review & editing, Visualization, Supervision, Investigation. **Didar Islam:** Writing – review & editing, Validation. **S.M. Shahriar Ahmed:** Formal analysis, Data curation. **Md Shamim Ahamed:** Writing – review & editing, Supervision. **Dara Shamsuddin:** Writing – review & editing, Validation, Investigation.

Data policy

The data will be made available upon reasonable request to the corresponding author.

Ethical statement

Hereby, I Nur Hussain consciously assure that for the manuscript ‘Spatiotemporal Dynamics of Carbon, Water, and Energy Balance in Bangladesh Using Multi-Source Remote Sensing and Climate Data’ the following is fulfilled:

1) All sources used are properly disclosed.
2) Ethical approval is not required for the use of the data in this research.
3) This material is the authors' own original work, which has not been previously published elsewhere.
4) The paper is not currently being considered for publication elsewhere.
5) The paper reflects the authors' own research and analysis in a truthful and complete manner.
6) The paper properly credits the meaningful contributions of co-authors and co-researchers.
7) Authors have no conflict of interest.
8) The authors declare that they have no financial interests or competing financial statements
9) The results are appropriately placed in the context of prior and existing research.
10) All authors have been personally and actively involved in substantial work leading to the paper and will take public responsibility for its content.

Funding information

This research was supported by CHINTA Research Bangladesh (CHINTA Research fund 2024).

Declaration of competing interest

The authors declare that they have no known competing financial interests or personal relationships that could have appeared to influence the work reported in this paper.

Acknowledgements

We acknowledge the MODIS Terra and Aqua satellites data provider (https://modis.gsfc.nasa.gov/data/), as well as energy flux data from NASA's LISD (https://disc.gsfc.nasa.gov/datasets/). Special thanks to the Bangladesh Meteorological Department (BMD) for providing national-scale meteorological data from 25 ground observatory weather stations. We also thank Department of Agricultural Extension, Dhaka, Bangladesh; Food and Agriculture Organization, Rome, Italy; Forest Department, Dhaka, Bangladesh; Bangladesh Space Research and Remote Sensing Organization (SPARRSO) and the International Union for Conservation of Nature (IUCN) for their crop calendar and phenological metrics knowledge-based resources. Our gratitude extends to McMaster University and the University of Toronto, Ontario, Canada, for providing access to MATLAB (Version R2024b) and ArcGIS-Pro (Version 3.4), which were essential for the analysis framework. Finally, we gratefully acknowledge CHINTA Research Bangladesh for providing the funding necessary for this research.

Appendix A. Data Interpolation and Regional Climate Patterns

Monthly precipitation and temperature data from 25 meteorological stations (Bangladesh Meteorological Department) were spatially interpolated using Inverse Distance Weighting (IDW) in ArcGIS Pro 3.4 to match the 500 m satellite data resolution. Station spacing ranged from 27 to 145 km (average 55 km), with statistical consistency maintained before and after interpolation. IDW produced continuous climate surfaces by weighting values according to proximity. Resulting temperature and precipitation maps are shown in Figure A1.

Bangladesh exhibits distinct seasonal and spatial climate patterns. Winter (December–February) temperatures are lowest (22–26 °C), especially in the north. March–May sees sharp warming, exceeding 34 °C in central and northwestern areas. The monsoon season (June–September) features moderate temperatures (26–34 °C) and heavy rainfall, peaking around 800 mm in the northeast and southeast due to orographic effects. The northwest remains hotter and drier, while coastal southern regions experience milder conditions year-round from maritime influences. These climatic gradients strongly influence regional environmental and agricultural dynamics.

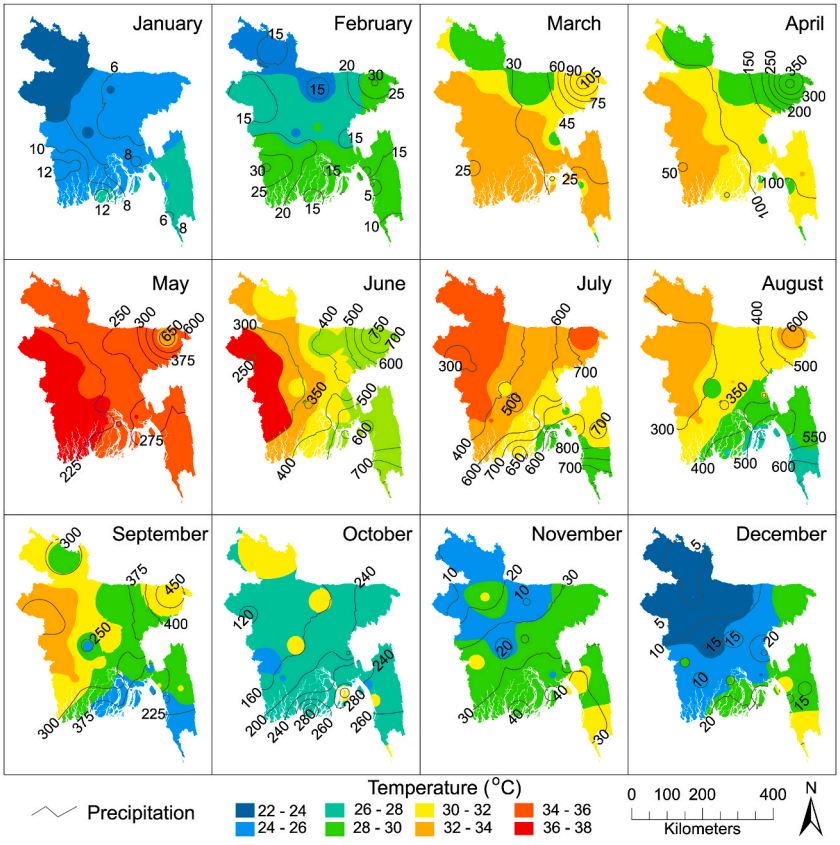

Fig. A1. (Appendix) Long-term average climate map of Bangladesh by month (January to December), where the color gradient represents the average temperature (°C) across the country from 2005 to 2022, and the lines indicate the monthly total precipitation (mm) during the same period.

Data availability

Data will be made available on request.

References

Acevedo-Siaca, L.G., Coe, R., Wang, Y., Kromdijk, J., Quick, W.P., Long, S.P., 2020. Variation in photosynthetic induction between rice accessions and its potential for improving productivity. New Phytol. 227 (4), 1097–1108.

Aguiar, R.G., De Musis, C.R., Aguiar, L.J.G., Martínez-Espinosa, M., Fischer, G.R., 2019. Energy balance closure in the Southwest Amazon forest site—a statistical approach. Theor. Appl. Climatol. 136, 1209–1219.

Ahmed, A.U., Siddiqi, N.A., Choudhuri, R.A., 1999. Vulnerability of forest ecosystems of Bangladesh to climate change. In: Vulnerability and Adaptation to Climate Change for Bangladesh. Dordrecht: Springer Netherlands, pp. 93–111.

Ai, Z., Wang, Q., Yang, Y., Manevski, K., Yi, S., Zhao, X., 2020. Variation of gross primary production, evapotranspiration and water use efficiency for global croplands. Agric. For. Meteorol. 287, 107935.

Al Mamun, M.A., Sarkar, M.A.R., Sarker, M.R., McKenzie, A.M., Nihad, S.A.I., Hossain, M.A., Hossain, A., 2025. Temperature variability and its effect on seasonal yield of rice in Bangladesh: a long-term trend assessment. Cogent Food Agric. 11 (1), 2447903.

Anjum, B., Sultana, R., Saddaf, N., 2024. The effectiveness of nature-based solutions to address climate change in Dhaka, Bangladesh. Soc. Sci. Humanit. Open 10, 100985.

Arsenault, K.R., Kumar, S.V., Geiger, J.V., Wang, S., Kemp, E., Mocko, D.M., et al., 2018. The land surface data toolkit (LDT v7. 2)–a data fusion environment for land data assimilation systems. Geosci. Model Dev. (GMD) 11 (9), 3605–3621.

Asner, G.P., Scurlock, J.M., Hicke, J.A., 2003. Global synthesis of leaf area index observations: implications for ecological and remote sensing studies. Global Ecol. Biogeogr. 12 (3), 191–205.

Ayers, J.M., Huq, S., 2009. The value of linking mitigation and adaptation: a case study of Bangladesh. Environ. Manag. 43, 753–764.

Azam, G., Huda, M.E., Bhuiyan, M.A.H., Mohinuzzaman, M., Bodrud-Doza, M., Islam, S.M.D., 2021. Climate change and natural hazards vulnerability of char land (bar land) communities of Bangladesh: application of the livelihood vulnerability index (LVI). Global Social Welf are 8, 93–105.

Baldocchi, D.D., Hincks, B.B., Meyers, T.P., 1988. Measuring biosphere-atmosphere exchanges of biologically related gases with micrometeorological methods. Ecology 69 (5), 1331–1340.

Bhatnagar, S., Chaudhary, R., Sharma, S., Janjhua, Y., Thakur, P., Sharma, P., Keprate, A., 2024. Exploring the dynamics of climate-smart agricultural practices for sustainable resilience in a changing climate. Environ. Sustain. Indic., 100535

Bhattacharya, B.K., Mallick, K., Desai, D., Bhat, G.S., Morrison, R., Clevery, J.R., et al., 2022. A coupled ground heat flux–surface energy balance model of evaporation using thermal remote sensing observations. Biogeosciences 19 (23), 5521–5551.

Bhowmik, J., Irfanullah, H.M., Selim, S.A., Budrudzaman, M., 2024. Assessing climate change-induced losses and damages to coastal ecosystem services: empirical evidence from Manpura Island, Bangladesh. Clim. Risk Manag. 45, 100641.

Bu, J., Gan, G., Chen, J., Su, Y., García, M., Gao, Y., 2021. Biophysical constraints on evapotranspiration partitioning for a conductance-based two source energy balance model. J. Hydrol. 603, 127179.

Burman, P.K.D., Sarma, D., Chakraborty, S., Karipot, A., Jain, A.K., 2020. The effect of Indian summer monsoon on the seasonal variation of carbon sequestration by a forest ecosystem over North-East India. SN Appl. Sci. 2 (2), 154.

Burman, P.K.D., Launiainen, S., Mukherjee, S., Chakraborty, S., Gogoi, N., Murkute, C., et al., 2021. Ecosystem-atmosphere carbon and water exchanges of subtropical evergreen and deciduous forests in India. For. Ecol. Manag. 495, 119371.

Burman, P.K.D., Chakraborty, S., Tiwari, Y.K., Sarma, D., Gogoi, N., 2024. Simulating the ecosystem-atmosphere carbon, water and energy fluxes at a subtropical Indian forest using an ecosystem model. Ecol. Model. 490, 110637.

Burman, P.K.D., Bhat, G.S., Tiwari, Y.K., Morrison, R., Rodda, S.R., Mukherjee, S., et al., 2025. Ecosystem-atmosphere exchanges of carbon dioxide, water vapour and energy in India: a synthesis of insights from eddy covariance measurements. Agric. For. Meteorol. 372, 110730.

Canadell, J.G., Monteiro, P.M., Costa, M.H., Cotrim da Cunha, L., Cox, P.M., Eliseev, A.V., et al., 2023. Intergovernmental Panel on climate change (IPCC). Global carbon and other biogeochemical cycles and feedbacks. In: Climate Change 2021: the Physical Science Basis. Contribution of Working Group I to the Sixth Assessment Report of the Intergovernmental Panel on Climate Change. Cambridge University Press, pp. 673–816.

Cao, R., Chen, Y., Shen, M., Chen, J., Zhou, J., Wang, C., Yang, W., 2018. A simple method to improve the quality of NDVI time-series data by integrating spatiotemporal information with the savitzky-golay filter. Rem. Sens. Environ. 217, 244–257.

Callejas-Rodelas, J.A., Knohl, A., Ramshorst, J.V., Mammarella, I., Markwitz, C., 2024. Comparison between lower-cost and conventional eddy covariance setups for CO2 and evapotranspiration measurements above monocropping and agroforestry systems. Agric. For. Meteorol. 354, 110086. https://doi.org/10.1016/j.agrformet.2024.110086.

Celis, J.A., Moreno, H.A., Basara, J.B., McPherson, R.A., Cosh, M., Ochsner, T., Xiao, X., 2021. From standard weather stations to virtual micro-meteorological towers in ungauged sites: modeling tool for surface energy fluxes, evapotranspiration, soil temperature, and soil moisture estimations. Remote Sens. 13 (7), 1271.

Celis, J., Xiao, X., Wagle, P., Basara, J., McCarthy, H., Souza, L., 2024. A comparison of moderate and high spatial resolution satellite data for modeling gross primary production and transpiration of native prairie, alfalfa, and winter wheat. Agric. For. Meteorol. 344, 109797.

Central Intelligence Agency, 2025. Bangladesh. The World Factbook. Retrieved. https://www.cia.gov/the-world-factbook/countries/bangladesh/. (Accessed 13 November 2021).

Chen, J.M., Liu, J., 2020. Evolution of evapotranspiration models using thermal and shortwave remote sensing data. Rem. Sens. Environ. 237, 111594.

Chu, H., Luo, X., Ouyang, Z., Chan, W.S., Dengel, S., Biraud, S.C., et al., 2021. Representativeness of eddy-covariance flux footprints for areas surrounding AmeriFlux sites. Agric. For. Meteorol. 301, 108350.

Crippa, M., Guizzardi, D., Pagani, F., Banja, M., Muntean, M., Schaaf, E., Monforti-Ferrario, F., Becker, W.E., Quadrelli, R., Risquez Martin, A., Taghavi-Moharamli, P., Köykkä, J., Grassi, G., Rossi, S., Melo, J., Oom, D., Branco, A., San-Miguel, J., Manca, G., Pisoni, E., Vignati, E., Pekar, F., 2024. GHG Emissions of all World Countries. Publications Office of the European Union. https://doi.org/10.2760/4002897.

Das, L.C., Islam, A.M., Aktar, S., Sultana, F., 2024. Climate change challenges in Bangladesh. World 2430001, 26.

Dastour, H., Alam, M.M., Dewan, A., Hassan, Q.K., 2025. Evaluating climatic warming and the modulating effects of surface water and regional variables in Western Bangladesh. Results Eng., 103864

Davidson, E.A., Janssens, I.A., 2006. Temperature sensitivity of soil carbon decomposition and feedbacks to climate change. Nature 440 (7081), 165–173.

Delogu, E., Le Dantec, V., Mordelet, P., Ceschia, E., Aubinet, M., Buysse, P., Pattey, E., 2017. Improved methodology to quantify the temperature sensitivity of the soil heterotrophic respiration in croplands. Geoderma 296, 18–29.

Deng, C., Zhang, B., Cheng, L., Hu, L., Chen, F., 2019. Vegetation dynamics and their effects on surface water-energy balance over the three-North Region of China. Agric. For. Meteorol. 275, 79–90.

Di Gregorio, A., Jansen, L.J., 2005. Land Cover Classification System (LCCS): Classification Concepts and User Manual. FAO, Rome.

Didan, K., Munoz, A.B., Solano, R., Huete, A., 2015. MODIS Vegetation Index User's Guide (MOD13 Series), vol. 35. University of Arizona: Vegetation Index and Phenology Lab, pp. 2–33.

DoE (Department of Environment), 2023. First biennial update report of Bangladesh to the UNFCCC. Ministry of Environment, Forest and Climate Change, Bangladesh. https://unfccc.int/sites/default/files/resource/Updated%20BUR1%20Report_15_11_2023.pdf.

Dubey, N., Ghosh, S., 2023. CO2 fertilization enhances vegetation productivity and reduces ecological drought in India. Environ. Res. Lett. 18 (6), 064025.

Dusenge, M.E., Duarte, A.G., Way, D.A., 2019. Plant carbon metabolism and climate change: elevated CO 2 and temperature impacts on photosynthesis, photorespiration and respiration. New Phytol. 221 (1), 32–49.
D'Odorico, P., Laio, F., Porporato, A., Ridolfi, L., Rinaldo, A., Rodriguez-Iturbe, I., 2010. Ecohydrology of terrestrial ecosystems. Bioscience 60 (11), 898–907.
Elfarkh, J., Johansen, K., El Hajj, M.M., Almashharawi, S.K., McCabe, M.F., 2023. Evapotranspiration, gross primary productivity and water use efficiency over a high-density olive orchard using ground and satellite based data. Agric. Water Manag. 287, 108423.
Fathi-Taperasht, A., Shafizadeh-Moghadam, H., Sadian, A., Xu, T., Nikoo, M.R., 2023. Drought-induced vulnerability and resilience of different land use types using time series of MODIS-based indices. Int. J. Disaster Risk Reduct. 91, 103703.
Fattah, M.A., Gupta, S.D., Farouque, M.Z., Ghosh, B., Morshed, S.R., Chakraborty, T., et al., 2023. Spatiotemporal characterization of relative humidity trends and influence of climatic factors in Bangladesh. Heliyon 9 (9), e19991.
Feng, M., Huang, C., Channan, S., Vermote, E.F., Masek, J.G., Townshend, J.R., 2012. Quality assessment of landsat surface reflectance products using MODIS data. Comput. Geosci. 38 (1), 9–22.
Feng, J., Wang, J., Song, Y., Zhu, B., 2018. Patterns of soil respiration and its temperature sensitivity in grassland ecosystems across China. Biogeosciences 15 (17), 5329–5341.
Frank, D., Reichstein, M., Bahn, M., Thonicke, K., Frank, D., Mahecha, M.D., et al., 2015. Effects of climate extremes on the terrestrial carbon cycle: concepts, processes and potential future impacts. Glob. Change Biol. 21 (8), 2861–2880.
Gebrechorkos, S.H., Peng, J., Dyer, E., Miralles, D.G., Vicente-Serrano, S.M., Funk, C., et al., 2023. Global high-resolution drought indices for 1981–2022. Earth Syst. Sci. Data Discuss. 2023, 1–28.
Govind, A., Kumari, J., 2014. Understanding the terrestrial carbon cycle: an ecohydrological perspective. Int. J. Ecol. 2014 (1), 712537.
Gower, S.T., Kucharik, C.J., Norman, J.M., 1999. Direct and indirect estimation of leaf area index, fAPAR, and net primary production of terrestrial ecosystems. Rem. Sens. Environ. 70 (1), 29–51.
Guan, X., Chen, J.M., Shen, H., Xie, X., 2021. A modified two-leaf light use efficiency model for improving the simulation of GPP using a radiation scalar. Agric. For. Meteorol. 307, 108546.
Heimann, M., Reichstein, M., 2008. Terrestrial ecosystem carbon dynamics and climate feedbacks. Nature 451 (7176), 289–292.
Hussain, N., Islam, M.N., 2020. Hot spot (G i*) model for forest vulnerability assessment: a remote sensing-based geo-statistical investigation of the Sundarbans mangrove forest, Bangladesh. Modeling Earth Systems and Environment 6 (4), 2141–2151.
Hussain, N., Firdaus, F., Rizwan, M., 2021. Remote sensing of photosynthesis, vegetation productivity and climate variability in Bangladesh. In: Re-envisioning Remote Sensing Applications. CRC Press, pp. 151–168.
Hussain, N., Arain, M.A., Wang, S., Parker, W.C., Elliott, K.A., 2024a. Evaluating the effectiveness of different variable retention harvesting treatments on forest carbon uptake using remote sensing. Remote Sens. Appl.: Society and Environment 33, 101124.
Hussain, N., Gonsamo, A., Wang, S., Arain, M.A., 2024b. Assessment of spongy moth infestation impacts on forest productivity and carbon loss using the Sentinel-2 satellite remote sensing and eddy covariance flux data. Ecol. Process. 13 (1), 37.
Hussain, N., Saifuzzaman, M., Alam, M., Ahamed, M.S., 2025. Assessing the impact of Long-term drought on agriculture in Bangladesh using multisource remote sensing data. Earth Systems and Environment 1–24.
Hussain, N., Rahman, M.A., Rakib, M.R., Islam, M.N., Kamruzzaman, M., 2026. Impact of drought on agricultural ecosystems, biomass and carbon uptake in the northern part of Bangladesh using remote sensing and weather station data. Remote Sensing in Earth Systems Sciences 9 (1), 14.
Isik, M.S., Parente, L., Consoli, D., Sloat, L., Mesquita, V., Ferreira, L.G., et al., 2025. Light Use Efficiency (LUE) Based Bimonthly Gross Primary Productivity (GPP) for Global Grasslands at 30 M Spatial Resolution (2000-2022).
Islam, M.S., Samreth, S., Islam, A.H.M.S., Sato, M., 2022. Climate change, climatic extremes, and households' food consumption in Bangladesh: a longitudinal data analysis. Environ. Chall. 7, 100495.
Islam, M.T., Nursey-Bray, M., 2017. Adaptation to climate change in agriculture in Bangladesh: the role of formal institutions. J. Environ. Manag. 200, 347–358.
Islam, S.M.D., Bhuiyan, M.A.H., Ramanathan, A.L., 2015. Climate change impacts and vulnerability assessment in coastal region of Bangladesh: a case study on shyamnagar upazila of Satkhira district. J. Clim. Change 1 (1–2), 37–45.
Ito, A., 2019. Disequilibrium of terrestrial ecosystem CO 2 budget caused by disturbance-induced emissions and non-CO 2 carbon export flows: a global model assessment. Earth Syst. Dyn. 10 (4), 685–709.
Jihan, M.A.T., Popy, S., Kayes, S., Rasul, G., Maowa, A.S., Rahman, M.M., 2025. Climate change scenario in Bangladesh: historical data analysis and future projection based on CMIP6 model. Sci. Rep. 15 (1), 7856.
Jung, M., Schwalm, C., Migliavacca, M., Walther, S., Camps-Valls, G., Koirala, S., et al., 2020. Scaling carbon fluxes from eddy covariance sites to globe: synthesis and evaluation of the FLUXCOM approach. Biogeosciences 17 (5), 1343–1365.
Kalma, J.D., 1972. The radiation balance of a tropical pasture, II. Net all-wave radiation. Agric. Meteorol. 10, 261–275.
Keenan, T.F., Williams, C.A., 2018. The terrestrial carbon sink. Annu. Rev. Environ. Resour. 43 (1), 219–243.
Khan, M.N.I., Azad, M.S., Hasan, T., Prova, A.F., Islam, M.S., Islam, M.R., Mollick, A.S., 2024. Structural diversity and carbon stocks in a tropical semi-evergreen forest in Bangladesh. Trees, Forests and People 16, 100534.
Khursheed, K., Imran, M., Ahmad, N., O'Nils, M., 2013. Efficient data reduction techniques for remote applications of a wireless visual sensor network. Int. J. Adv. Rob. Syst. 10 (5), 240.
Kondo, M., Saitoh, T.M., Sato, H., Ichii, K., 2017. Comprehensive synthesis of spatial variability in carbon flux across monsoon Asian forests. Agric. For. Meteorol. 232, 623–634.
Krause, A., Papastefanou, P., Gregor, K., Layritz, L.S., Zang, C.S., Buras, A., et al., 2022. Quantifying the impacts of land cover change on gross primary productivity globally. Sci. Rep. 12 (1), 18398.
Kutner, M.H., Nachtsheim, C., Neter, J., Li, W., 2004. Applied Linear Statistical Models. McGraw-Hill. https://doi.org/10.1036/0072386886.
Lee, H., Calvin, K., Dasgupta, D., Krinner, G., Mukherji, A., Thorne, P., et al., 2024. CLIMATE CHANGE 2023 synthesis report summary for policymakers. CLIMATE CHANGE 2023 Synthesis Report: Summary for Policymakers.
Li, X., Xiao, J., 2019. Mapping photosynthesis solely from solar-induced chlorophyll fluorescence: a global, fine-resolution dataset of gross primary production derived from OCO-2. Remote Sens. 11 (21), 2563.
Liang, S., Wang, D., 2017. Moderate resolution imaging spectroradiometer (MODIS) downward shortwave radiation (MCD18A1) and photosynthetically active radiation (MCD18A2) algorithm theoretical basis document. https://modis-land.gsfc.nasa.gov/pdf/mcd18_user_guide_C61_v3.pdf.
Liu, X., Feng, X., Fu, B., 2020. Changes in global terrestrial ecosystem water use efficiency are closely related to soil moisture. Sci. Total Environ. 698, 134165.
Liu, H., Rezanezhad, F., Zhao, Y., He, H., Van Cappellen, P., Lennartz, B., 2024. The apparent temperature sensitivity (Q10) of peat soil respiration: a synthesis study. Geoderma 443, 116844.
Ma, Y., Guan, X., Wang, Y., Li, Y., Lin, D., Shen, H., 2025. GPP estimation by transfer learning with combined solar-induced chlorophyll fluorescence and eddy covariance data. Int. J. Appl. Earth Obs. Geoinf. 139, 104503.
Majumder, S.C., Islam, K., Hossain, M.M., 2019. State of research on carbon sequestration in Bangladesh: a comprehensive review. Geology, Ecology, and Landscapes 3 (1), 29–36.
Malhi, Y., Franklin, J., Seddon, N., Solan, M., Turner, M.G., Field, C.B., Knowlton, N., 2020. Climate change and ecosystems: threats, opportunities and solutions. Philos. Trans. R. Soc. B 375 (1794), 20190104.
Marcolla, B., Migliavacca, M., Rödenbeck, C., Cescatti, A., 2020. Patterns and trends of the dominant environmental controls of net biome productivity. Biogeosciences 17 (8), 2365–2379.
Migliavacca, M., Musavi, T., Mahecha, M.D., Nelson, J.A., Knauer, J., Baldocchi, D.D., et al., 2021. The three major axes of terrestrial ecosystem function. Nature 598 (7881), 468–472.

Monteith, J.L., 1965. Evaporation and environment. In: Symposia of the Society for Experimental Biology, vol. 19. Cambridge University Press (CUP, Cambridge, pp. 205–234.
Monteith, J.L., 1972. Solar radiation and productivity in tropical ecosystems. J. Appl. Ecol. 9 (3), 747–766.
Nagele, P., 2003. Misuse of standard error of the mean (SEM) when reporting variability of a sample. A critical evaluation of four anaesthesia journals. Br. J. Anaesth. 90 (4), 514–516.
Novák, V., Novák, V., 2012. Evapotranspiration: a component of the water cycle. Evapotranspiration in the soil-plant-atmosphere System, pp. 1–13.
Nzabarinda, V., Bao, A., Tie, L., Uwamahoro, S., Kayiranga, A., Ochege, F.U., Muhirwa, F., Bao, J., 2025. Expanding forest carbon sinks to mitigate climate change in Africa. Renew. Sustain. Energy Rev. 207, 114849. https://doi.org/10.1016/j.rser.2024.114849.
Olken, F., Rotem, D., 1995. Random sampling from databases: a survey. Stat. Comput. 5, 25–42.
Pei, Y., Dong, J., Zhang, Y., Yuan, W., Doughty, R., Yang, J., et al., 2022. Evolution of light use efficiency models: improvement, uncertainties, and implications. Agric. For. Meteorol. 317, 108905.
Penman, H.L., 1948. Natural evaporation from open water, bare soil and grass. Proc. Roy. Soc. Lond. Math. Phys. Sci. 193 (1032), 120–145.
Penman, H.L., 1963. Vegetation and hydrology. Soil Sci. 96 (5), 357.
Pereira, L.F., Fernandes-Filho, E.I., Gomes, L.C., Arruda, D.M., Oliveira, G.C., Schaefer, C.E.G.R., et al., 2024. Soil and vegetation types are predisposition factors controlling greenness changes: a shift of paradigm in greening and browning modelling? Remote Sens. Appl.: Society and Environment 36, 101366.
Pugnaire, F.I., Morillo, J.A., Peñuelas, J., Reich, P.B., Bardgett, R.D., 2019. Climate change effects on plant-soil feedbacks and consequences for biodiversity and functioning of terrestrial ecosystems. Sci. Adv. 5 (11).
Quetin, G.R., Famiglietti, C.A., Dadap, N.C., Bloom, A.A., Bowman, K.W., Diffenbaugh, N.S., et al., 2023. Attributing past carbon fluxes to CO2 and climate change: respiration response to CO2 fertilization shifts regional distribution of the carbon sink. Glob. Biogeochem. Cycles 37 (2) e2022GB007478.
Rahman, L.M., 2016. Forest Resources. *Bangladesh National Conservation Strategy*. Government of the People's Republic of Bangladesh, pp. 2–13.
Rahman, M.A., Kang, S., Nagabhatla, N., Macnee, R., 2017. Impacts of temperature and rainfall variation on rice productivity in major ecosystems of Bangladesh. Agric. Food Secur. 6, 1–11.
Rahman, S., Anik, A.R., 2020. Productivity and efficiency impact of climate change and agroecology on Bangladesh agriculture. Land Use Policy 94, 104507.
Reid, H., Shafiqul Alam, S., 2017. Ecosystem-based approaches to adaptation: evidence from two sites in Bangladesh. Clim. Dev. 9 (6), 518–536.
Ritchie, H., Roser, M., Rosado, P., 2020. CO_2 and greenhouse gas emissions. Our World in Data. https://ourworldindata.org/co2/country/bangladesh. (Accessed 20 December 2024).
Rodda, S.R., Thumaty, K.C., Praveen, M.S.S., Jha, C.S., Dadhwal, V.K., 2021. Multi-year eddy covariance measurements of net ecosystem exchange in tropical dry deciduous forest of India. Agric. For. Meteorol. 301, 108351.
Röll, A., Marques, I., Ramadhani, D.N., Valdes-Uribe, A., Hendrayanto, H., Hölscher, D., 2024. Changes in leaf area index by tropical forest transformation to plantations increase below-canopy surface temperatures. Glob. Ecol. Conserv., e03001
Rotenberg, E., Tatarinov, F., Muller, J.D., Yakir, D., 2025. Evapotranspiration saturation amplifies climate sensitivity of terrestrial water yield. Nat. Commun.
Roxburgh, S.H., Berry, S.L., Buckley, T.N., Barnes, B., Roderick, M.L., 2005. What is NPP? Inconsistent accounting of respiratory fluxes in the definition of net primary production. Funct. Ecol. 19 (3), 378–382.
Running, S.W., Nemani, R.R., Heinsch, F.A., Zhao, M., Reeves, M., Hashimoto, H., 2004. A continuous satellite-derived measure of global terrestrial primary production. Bioscience 54 (6), 547–560.
Running, S.W., Mu, Q., Zhao, M., Moreno, A., 2019. MODIS global terrestrial evapotranspiration (ET) product (MOD16A2/A3 and year-end gap-filled MOD16A2GF/A3GF, National Aeronautics and Space Administration, Washington, DC, USA. https://doi.org/10.5067/MODIS/MOD16A2,6. NASA Earth Observing System MODIS Land Algorithm (For Collection 6).
Sauer, T.J., Singer, J.W., Prueger, J.H., DeSutter, T.M., Hatfield, J.L., 2007. Radiation balance and evaporation partitioning in a narrow-row soybean canopy. Agric. For. Meteorol. 145 (3–4), 206–214.
Saini, A., Sahu, N., Kumar, P., Nayak, S., Duan, W., Avtar, R., Behera, S., 2020. Advanced rainfall trend analysis of 117 years over west coast plain and hill agro-climatic region of India. Atmosphere 11 (11), 1225.
See, C.R., Virkkala, A.M., Natali, S.M., Rogers, B.M., Mauritz, M., Biasi, C., et al., 2024. Decadal increases in carbon uptake offset by respiratory losses across northern permafrost ecosystems. Nat. Clim. Change 14 (8), 853–862.
Sett, T., Nandy, S., Patel, N.R., Padalia, H., Srinet, R., Watham, T., 2023. Spatio-temporal dynamics of water use efficiency over forest ecosystems using time series satellite data and carbon flux measurements. For. Ecol. Manag. 548, 121385.
Seneviratne, S.I., Zhang, X., Adnan, M., Badi, W., Dereczynski, C., Luca, A.D., et al., 2021. Weather and climate extreme events in a changing climate. Climate Change 2021 – the Physical Science Basis Working Group I Contribution to the Sixth Assessment Report of the Intergovernmental Panel on Climate Change (IPCC). Cambridge University Press, Cambridge, United Kingdom and New York, NY, USA, pp. 1513–1766. https://doi.org/10.1017/9781009157896.013.
Seleiman, M.F., Al-Suhaibani, N., Ali, N., Akmal, M., Alotaibi, M., Refay, Y., et al., 2021. Drought stress impacts on plants and different approaches to alleviate its adverse effects. Plants 10 (2), 259.
Sepulcre-Canto, G., Vogt, J., Arboleda, A., Antofie, T., 2014. Assessment of the EUMETSAT LSA-SAF evapotranspiration product for drought monitoring in Europe. Int. J. Appl. Earth Obs. Geoinf. 30, 190–202.
Sharma, N., Raman, H., Wheeler, D., Kalenahalli, Y., Sharma, R., 2023. Data-driven approaches to improve water-use efficiency and drought resistance in crop plants. Plant Sci. 336, 111852.
Shewhart, W.A., Wilks, S.S., Balding, D.J., Bloomfield, P., Cressie, N.A.C., Fisher, N.I., Johnstone, I.M., Kadane, J.B., Ryan, L.M., Scott, D.W., et al., 2003. Wiley Series in Probability and Statistics. Wiley, New York, USA.
Smith, P., Ashmore, M.R., Black, H.I., Burgess, P.J., Evans, C.D., Quine, T.A., et al., 2013. The role of ecosystems and their management in regulating climate, and soil, water and air quality. J. Appl. Ecol. 50 (4), 812–829.
Suepa, T., Qi, J., Lawawirojwong, S., Messina, J.P., 2016. Understanding spatio-temporal variation of vegetation phenology and rainfall seasonality in the monsoon Southeast Asia. Environ. Res. 147, 621–629.
Sun, Y., Peng, D., Guan, X., Chu, D., Ma, Y., Shen, H., 2023. Impacts of the data quality of remote sensing vegetation index on gross primary productivity estimation. GIScience Remote Sens. 60 (1), 2275421.
Tadese, S., Soromessa, T., Aneseye, A.B., Gebeyehu, G., Noszczyk, T., Kindu, M., 2023. The impact of land cover change on the carbon stock of moist afromontane forests in the Majang forest biosphere reserve. Carbon Bal. Manag. 18, 24. https://doi.org/10.1186/s13021-023-00243-z.
Tithi, A.C., Sohel, M.S.I., Jakariya, M., Rana, P., 2024. Analyzing ecosystem functions in Bangladesh's forests: a historical MODIS study. Geology, Ecology, and Landscapes 1–13.
United States Geological Survey, 2021. Generalized physiographic map of Bangladesh (physio8bg). U.S. Geological Survey data release. https://doi.org/10.5066/P9BP7233. (Accessed 21 May 2021).
Van Oijen, M., Schapendonk, A., Höglind, M., 2010. On the relative magnitudes of photosynthesis, respiration, growth and carbon storage in vegetation. Ann. Bot. 105 (5), 793–797.
Vicente-Serrano, S.M., Camarero, J.J., Olano, J.M., Martín-Hernández, N., Peña-Gallardo, M., Tomás-Burguera, M., et al., 2016. Diverse relationships between forest growth and the normalized difference vegetation index at a global scale. Rem. Sens. Environ. 187, 14–29.
Wan, Z., 2006. MODIS land surface temperature products users' guide. In: Institute for Computational Earth System Science, 805. University of California, Santa Barbara, CA, USA, p. 26.
Wang, C., Yang, J., Zhang, Q., 2006. Soil respiration in six temperate forests in China. Glob. Change Biol. 12 (11), 2103–2114.
Wang, J., Jiang, F., Wang, H., Qiu, B., Wu, M., He, W., et al., 2021. Constraining global terrestrial gross primary productivity in a global carbon assimilation system with OCO-2 chlorophyll fluorescence data. Agric. For. Meteorol. 304, 108424.
Wang, T., Zhang, Y., Yue, C., Wang, Y., Wang, X., Lyu, G., et al., 2024. Progress and challenges in remotely sensed terrestrial carbon fluxes. Geo-Spatial Inf. Sci. 1–21.

Wang, Y.P., Zhang, L., Liang, X., Yuan, W., 2024. Coupled models of water and carbon cycles from leaf to global: a retrospective and a prospective. Agric. For. Meteorol. 358, 110229.
Wei, Q., Xue, L., Jia, Z., Chen, Y., Chen, P., 2025. Assessing net primary productivity variation and potential future impacts based on machine learning and contribution analysis in the yangtze river Delta, China. Sci. Total Environ. 989, 179886.
Weiland, L., Rogers, C.A., Sothe, C., Arain, M.A., Gonsamo, A., 2023. Satellite-based land surface temperature and soil moisture observations accurately predict soil respiration in temperate deciduous and coniferous forests. Agric. For. Meteorol. 340, 109618.
White, M.A., Hoffman, F., Hargrove, W.W., Nemani, R.R., 2005. A global framework for monitoring phenological responses to climate change. Geophys. Res. Lett. 32 (4).
Wilson, K.B., Baldocchi, D.D., Aubinet, M., Berbigier, P., Bernhofer, C., Dolman, H., et al., 2002. Energy partitioning between latent and sensible heat flux during the warm season at FLUXNET sites. Water Resour. Res. 38 (12), 30–31.
Xue, J., Su, B., 2017. Significant remote sensing vegetation indices: a review of developments and applications. J. Sens. 2017 (1), 1353691.
Yang, D., Xu, X., Xiao, F., Xu, C., Luo, W., Tao, L., 2021. Improving modeling of ecosystem gross primary productivity through re-optimizing temperature restrictions on photosynthesis. Sci. Total Environ. 788, 147805.
Yang, J., Lu, X., Liu, Z., Tang, X., Yu, Q., Wang, Y., 2024. Atmospheric drought dominates changes in global water use efficiency. Sci. Total Environ. 934, 173084.
Yang, S., Zhang, J., Han, J., Wang, J., Zhang, S., Bai, Y., et al., 2021. Evaluating global ecosystem water use efficiency response to drought based on multi-model analysis. Sci. Total Environ. 778, 146356.
Yang, Y., Guan, H., Batelaan, O., McVicar, T.R., Long, D., Piao, S., et al., 2016. Contrasting responses of water use efficiency to drought across global terrestrial ecosystems. Sci. Rep. 6 (1), 23284.
Yang, Y., Shi, Y., Sun, W., et al., 2022. Terrestrial carbon sinks in China and around the world and their contribution to carbon neutrality. Sci. China Life Sci. 65, 861–895.
Yuan, Q., Wang, X., Che, T., Li, J., 2025. Global carbon flux dataset generated by fusing remote sensing and multiple flux networks observation. Sci. Data 12 (1), 1359.
Zakariazadeh, A., Ahshan, R., Al Abri, R., Al-Abri, M., 2024. Renewable energy integration in sustainable water systems: a review. Clean. Eng. Technol., 100722
Zhang, S., Liu, T., Duan, L., Hao, L., Tong, X., Jia, T., Li, X., Lun, S., 2024. Characterization and drivers of water and carbon fluxes dynamics in dune ecosystems of the Horqin Sandy land. Sci. Total Environ. 918, 170517. https://doi.org/10.1016/j.scitotenv.2024.170517.
Zhang, X., Friedl, M.A., Schaaf, C.B., Strahler, A.H., Hodges, J.C., Gao, F., et al., 2003. Monitoring vegetation phenology using MODIS. Rem. Sens. Environ. 84 (3), 471–475.
Zhang, Y., Xiao, X., Wu, X., Zhou, S., Zhang, G., Qin, Y., Dong, J., 2017. A global moderate resolution dataset of gross primary production of vegetation for 2000–2016. Sci. Data 4 (1), 1–13.
Zhang, Z., Zhang, Y., Zhang, Y., Gobron, N., Frankenberg, C., Wang, S., Li, Z., 2020. The potential of satellite FPAR product for GPP estimation: an indirect evaluation using solar-induced chlorophyll fluorescence. Rem. Sens. Environ. 240, 111686.
Zhao, J., Liu, D., Cao, Y., Zhang, L., Peng, H., Wang, K., Xie, H., Wang, C., 2022. An integrated remote sensing and model approach for assessing forest carbon fluxes in China. Sci. Total Environ. 811, 152480. https://doi.org/10.1016/j.scitotenv.2021.152480.
Zhu, L., Song, R., Sun, S., Li, Y., Hu, K., 2022. Land use/land cover change and its impact on ecosystem carbon storage in coastal areas of China from 1980 to 2050. Ecol. Indic. 142, 109178.
Zhu, S., Xu, J., Zeng, J., Feng, X., Wang, Y., Bao, S., Shi, J., 2023. Explainable machine learning confirms the global terrestrial CO 2 fertilization effect from space. IEEE Geoscience and Remote Sensing Letters 20, 1–5.
Zhu, S., Xu, J., Zeng, J., He, P., Wang, Y., Bao, S., et al., 2024. UFLUX-GPP: a cost-effective framework for quantifying daily terrestrial ecosystem carbon uptake using satellite data. IEEE Trans. Geosci. Rem. Sens.